Surface-Weighted Gaussian-Moment Method for Polydisperse Multiphase Flow Prediction

by

Mathieu Marchildon

A thesis submitted in conformity with the requirements
for the degree of Master of Applied Science

Department of Mechanical Engineering
University of Ottawa

Surface-Weighted Gaussian-Moment Method for Polydisperse Multiphase Flow Prediction

Mathieu Marchildon
Master of Applied Science

Department of Mechanical Engineering
University of Ottawa
2023

Abstract

Polydisperse multiphase flows are characterized as particle-laden flows, for which the flows of interest are comprised of small particles of different sizes. These flows are computationally difficult to model as the number of particles increases. As such, many methods have been developed over the years in order to build simplified models. One such technique, higher-order moment closure methods, provide an expanded set of partial differential equations (PDEs) describing the evolution of statistical properties of the particle phase. Moment-based methods rely on modelling the statistical moments of the studied flow, such as the average particle velocity and provides equations describing the evolution of these moments. This thesis introduces the fundamentals of kinetic theory and moment methods, provides an extension to a previously proposed three-dimensional polydisperse Gaussian-moment model (PGM). The previous PGM, while showing promising preliminary results, has been improved by the implementation of surface-weighted particle statistics. Namely this new model exactly recovers the steady-state solution for particles settling in Stokes flow. Finally, this thesis describes the numerical methods used in obtaining one-dimensional and three-dimensional results of the PGM. Several simple flow problems are solved and analysed to demonstrate the predictive capabilities of the new model.

Acknowledgments

This study was funded by the Natural Science and Engineering Research Council of Canada (NSERC) through grant number RGPIN-2020-06295 and by the Atomic Energy of Canada Limited, under the auspices of the Federal Nuclear Science and Technology Program. The research was conducted in conjunction with the Canadian Nuclear Laboratories. Computational resources for this work were provided by the Argonne Leadership Computing Facility (ALCF) and the Niagara supercomputer at the SciNet HPC Consortium. The ALCF is a DOE Office of Science User Facility supported under Contract DE-AC02-06CH11357. The SciNet HPC consortium is funded by the Canada Foundation for Innovation; the Government of Ontario; Ontario Research Fund - Research Excellence; and the University of Toronto. A huge thanks is in order to Benoît Allard who provided useful corrections and improvement to the presented model.

and my 4 core Intel i5-7600K CPU @ 3.80GHz . . . the little engine that could.

Ottawa 2020-2022

Contents

List of Tables

List of Figures

Chapter 1

Introduction

Polydisperse multiphase flows are characterized as a specialized type of multiphase flow. These flows are comprised of numerous small particles suspended in a background fluid. Such flows appear ubiquitously and are present in myriad practical engineering applications, such as in fluidization applications or in the use of aerosol sprays. Theses flows contain very small particles that play a role in the development of the flow. Modelling the evolution of these particles and their effect on the flow during these events remains computationally difficult. Applying a Lagrangian approach is often computationally unfeasible as the number of particles increase, making a Lagrangian approaches for physical simulations for many practical situations extremely expensive. Eulerian formulations have been proposed as an alternative modelling technique. While these formulations are often less computationally expensive to preform than traditional Lagrangian models, they come with their own set of issues. Namely, Eulerian models often produce mathematical artifacts, such as the inability to model a stream of particles crossing, or other issues that occur when dealing with fluid boundary problems [20]. One family of Eulerian models is the moment-based methods [5, 17, 6, 31]. In these models, the evolution of the statistical moments of the fluid are tracked in order to develop an understanding of the flow. These moments are typically related to observable field properties of the studied fluid and are also referred to as the macroscopic properties of the fluid. The evolution of the macroscopic properties, such as the average velocity of the particles contains useful information in building an understanding of the development of the fluid.

1.1 Motivation and Objectives

Recently, Forgues *et al.* [5] have proposed a fifteen-moment polydisperse Gaussian-moment model (PGM) for modelling polydisperse multiphase flows. The fifteen-moment PGM provides an attractive treatment for polydisperse flows, as a set of first-order hyperbolic balance laws are obtained that provide useful statistical properties of the flow that are not normally captured in traditional Eulerian models. Information obtained from the model, such as the local variance of the particles velocity with respect to its size can be very useful in developing an understanding of the development of the flow and the impact polydisperse particles can have on such flows. Though

the model proved to be accurate in many regimes, the fifteen-moment PGM fails to recover the exact steady-state solution for particles settling in a Stokes flow [5]. Being able to recover the exact steady-state solution is of significant interest when studying polydisperse flows such as those present in aerosol sprays or atmospherics pollutants, as knowing the settling particle velocity and location is normally what these models are trying to predict. For instance, since the start of the COVID-19 pandemic in 2019, a recent interest has been placed into the research and development of models attempting to model particle dispersion present in coughs in order to accurately predict the dispersion of viral droplets in the atmosphere. Advanced polydisperse models would provide researchers with the tools to develop adequate personal protective equipment and test various methods such as ventilation systems in order to contain or reduce the viral load circulating in the atmosphere. Such computer models, if proven to be sufficiently reliable, would be able to eliminate or at the very least reduce the need to preform costly and time extensive laboratory tests. In addition, another advantage of reliable models is that they can be configured to account for various environments such that these models can be used to obtain results for dynamic and ever changing situations. The continued development of polydisperse models will reduce the work load placed on such research fields and increase the capabilities to quickly respond to dynamic and changing situations.

The newly-proposed surface-based PGM in this work is an extended version of the previous PGM that allows one to capture the exact steady-state solution for settling flows. Furthermore, the fifteen-moment PGM has also been extended to account for particle evaporation by providing additional flexibility into the treatment of flows with additional external effects. Capturing particle evaporation in the PGM extends the range of application to include polydisperse flows present in various applications such as the dispersion of aerosol droplets generated by sprays or violent respiratory events (*e.g.*, coughing). In these situations, not only is there a need to track the location of the particles during the evolution and at steady state but evaporation, namely in the case of violent respiratory events where evaporation plays a significant role in the dispersion of the particles. In addition to the surface-based PGM, an exact kinetic solver was developed in order to compare the results obtained from the PGM to the known kinetic solution. This exact kinetic solver is designed to be efficient and highly-scalable on distributed computing systems, such that moments of any provided set of kinetic equations can be easily computed.

1.2 Research Outline

The content of this thesis is structured as follows. Chapter 2 provides a background to multiphase flows and various approaches one can take in order to develop an effective treatment of multiphase flows. Chapter 3 introduces the fundamental ideas of kinetic theory of gases and how the basic ideas of kinetic theory can be applied to polydisperse multiphase flows. This section sets forth the fundamentals of kinetic theory from which the PGM is built upon. In Chapter 4, the new polydisperse Gaussian model is derived along with the source term that is considered for the model. Chapter 5 outlines the mathematical principles used in the implementation of the

exact moment solver. Finally, in Chapter 7, numerical results of the PGM are shown. These results are used to demonstrate the capabilities of the new polydisperse Gaussian model by first presenting a space-homogeneous case and recovery of the steady-state solution. Furthermore, a space-homogeneous case with evaporation in addition to a three-dimensional simulations are shown in order to showcase the capabilities of the PGM in handling more complex polydisperse multiphase problems.

1.2.1 Scope of Work

While the field of multiphase flows is diverse, such that there are many approaches one can take to build models in order to accurately predict polydisperse multiphase flows, this thesis main focus is in the development and expansion of the family of PGM based models. As such this thesis takes on a theoretical approach in the treatment of mulitphase flows. Many assumptions, that one might deem incorrect in any treatment of multiphase flows for any practical engineering applications are taken in this thesis. Many of theses assumptions that stem from the fundamentals of kinetic theory of gases (outlined in Chapter 3) and specific assumptions to the development of the PGM in Chapter 4 might be deemed inappropriate for any practical treatment of multiphase flows. One such assumption is neglecting particle collisions. As is outlined in the following sections particle collisions are not considered for the scope of this thesis. In any practical engineering applications for modelling multiphase flows, namely situations such as sprays, particle collisions play a significant role in the development of the flow. It can be argued that neglecting particle collisions in the PGM invalidate the model for any practical engineering applications. But as previously mentioned this thesis serves to lay the foundational work for the expansion of the PGM family of models. As such the scope of this thesis is limited to the treatment of the moments in their simplified form with a simplified source term in order to validate the model. As the addition of particle collisions or the treatment of particles in various flow regimes come with additional complexity to the model that present additional modelling and numerical difficulties the scope of this thesis was limited to the treatment of the moments of the PGM family of models.

As the PGM family of models is still in its early stages of development it is important to build the foundational work and the appropriate approach for treatment of multiphase flows with moment-based methods. It is to be noted that the derivation and expansion of the PGM family of models in this work was done in such a way such that future work can build upon the fundamentals presented in this thesis. Most notably the inclusion of treatment of various flow regimes, or consideration of particle collisions can be integrated into the model via modification of the initial assumptions presented in Chapter 4. Modifications of these assumptions will most-likely lead to alternative source terms than the ones present in this thesis yet treatment of moments will remain very similar to the ones derived in this thesis.

Chapter 2

Multiphase Flows

Depending of the situation one might find themselves in, different approaches to model the multiphase flows might be better suited than others. For instance, traditional Eulerian models fair very well when the particle phase is tightly coupled to the fluid phase. In these situations the particle phase treatment can be performed in a similar fashion the fluid phase with the traditional Euler or Navier-Stokes equations. By comparison, at higher Stokes number, particles become detached from the carrier fluid and their behaviour can not be adequately described with traditional field based methods that assume the particle phase is tightly coupled to the fluid phase.

2.1 Description of Particles in Multiphase Flows

In order to adequately model particles present in multiphase flows it is important to develop an appropriate model for the particles and the forces present in the system. To begin, particles present in multiphase flows are often modelled as spheres composed of a uniform substance and expressed with a constant density. While this is not entirely true, this approximation greatly simplifies the models and, as such, is often used in treatments of multiphase flows. The mass of the particles can be easily equated to the radius of such particles as

$$m_p = \rho_p \frac{4}{3} \pi r^3 \,, \tag{2.1}$$

where m_p is the mass of the particle in question, ρ_p its density and r the radius. Particle collisions in multiphase flows can be modelled with varying levels of fidelity and complexity, for this work, the flows in question are assumed to be dispersed enough such that particle collisions do not have a significant effect on the development of the flow, collisions are therefore ignored.

Particle-laden flows, such as those studied in this work, can be characterized by their Stokes number. The Stokes number, St, is defined as

$$\mathrm{St} = \frac{\tau \, |V_i|}{l} \,, \tag{2.2}$$

where V_i is the speed of the background fluid, l is the characteristic length of the particles in the

flow and τ is a relaxation parameter of the particles in the system. The Stokes number of the flow helps to describe how strongly the particles in the system are affected by drag forces caused by the background fluid. In a system with a small Stokes number, such that $\mathrm{St} \ll 1$, particles in the system are strongly coupled to the background flow. This means particles in such flows closely follow the background flow and are strongly and quickly affected by any changes in the background flow. Additionally, particles in the system are within a similar range of velocities, that of the background flow. When the Stokes number is very large, $\mathrm{St} \gg 1$, the effect of the background flow on the particles velocities plays only a very small or negligible role in their overall velocity. When the Stokes number of the system in near one, particles are still affected by the background flow but the particles in the system can still admit a wide range of possible velocities. It is this intermediate regime that is often most difficult to model.

The flows studied in this work are assumed to follow a Stokes-flow approximation. The Stokes-flow approximation is valid for low Reynolds number, specifically $\mathrm{Re} < 1$, and can be useful to model drag forces on spherical particles in a background flow due to its direct relationship to the relaxation of particles. Acceleration of the particles due to drag, gravity, and buoyancy in the system can be described as

$$a_i = \frac{V_i - v_i}{\tau} + \phi_i \,. \tag{2.3}$$

In Eq. (2.3), v_i is velocity of the particles, τ is the corresponding relaxation rate of the particles due to drag forces and ϕ_i is the acceleration felt by the particles as a result of the gravitational and buoyancy forces in the system with respect to the fluid medium. For low Reynolds numbers, the relaxation felt by spherical particles can be expressed in terms of the particles surface area s, its density, ρ_p, and the fluids dynamic viscosity, μ_f, as

$$\tau = \frac{\rho_p s}{18\pi\mu_f} \,. \tag{2.4}$$

Additionally, the buoyancy of the particles, ϕ_i, can be expressed as a relationship between the particles density, ρ_p, and the fluids density, ρ_f, with the acceleration due to gravity g_i,

$$\phi_i = \frac{\rho_p - \rho_f}{\rho_p} g_i \,. \tag{2.5}$$

In addition to the drag forces acting on the particles in the system, another major component to be considered in multiphase flows is the possible evaporation of the particles contained within the flow. This evaporation plays a significant role in the outcome of the flow as the effect of particles evaporating in the system alters to total number density of the particles in the system. Furthermore, as the particle size changes over time due to evaporation, this has a compounding effect on the drag of the particles in the system as it is directly proportional to the surface area of the particles. For this work, a simple steady-state linear evaporation rate for spherical particles is used such that Υ, the rate of change of the particle surface area, given by

$$\Upsilon = -\alpha\pi \,, \tag{2.6}$$

where α is often tabulated for various fuels [3, 9, 14] . There exist many different models for particle evaporation, Eq. (2.6) will be used for the scope of this thesis as it provides a simple linear model that is commonly used in spray modelling.

2.2 Lagrangian Multiphase Models

Traditional Lagrangian models track the trajectories of the individual particles in the flow through the solution of ordinary differential equations (ODEs). These ODEs are often presented in the form

$$m_p \frac{\mathrm{d}v_i}{\mathrm{d}t} = \sum f_\alpha \,. \tag{2.7}$$

In Eq. (2.7), the mass and velocity vector of the particles, m_p and v_i, are equated to summation of all the forces present in the model. These forces often take on models for simple spherical particles, depending on the situation. The common forces considered in these models are often the ones that have the greatest impact on the development of the flow. These forces are often taken as buoyancy and drag. In these Lagrangian models the position vector, x_i, of the particles is obtained by integration of the velocity vector,

$$x_i = \int v_i \, \mathrm{d}t \,. \tag{2.8}$$

As previously stated, obtaining the position of each particle, with an increasing number of particles in the domain or consideration of additional external forces becomes increasingly difficult to preform numerically. In order to avoid having to numerically obtain the position of each individual particle in the flow, field-based models describing the evolution of the entire population of particles are often proposed.

2.2.1 Eulerian Multiphase Models

Another common way to handle multiphase flows is to take an Eulerian approach. As it is difficult to track individual particles one can find a way to describe groups of particles. The groups of particles, or fields can then be described using well known PDEs in order to model their evolution over time. One of the simplest field equations that can be used to describe particles in a flow would be a convection equation

$$\frac{\partial \rho}{\partial t} + V_i \frac{\partial \rho}{\partial x_i} = 0. \tag{2.9}$$

In this simplified convection model, the particle density, ρ, is modelled over time as it follows the carrier phase of the convection model in space, x_i. The speed of the carrier phase in Eq. (2.9) is then described by V_i.

An extension to this model would be to allow the particles in the field to have a different velocity from the background carrier phase [24]. Theses models, while computationally less intensive than tracking individual particles in the system, are significantly hindered by the assumption that at a single point in space particles can only admit a single velocity. Namely, when flows contain

a wide range of particle size such is the case in polydisperse flows and by consequence a wide range of velocities many modelling artifacts appear due to the nature of field assumptions being unable to describe particles containing varying velocities at a single point in space.

2.2.2 Moment-Based Multiphase Models

The model in this work presents a Eularian moment-based model for treatment of multiphase flows. These moment-based models are a natural extension to the Eularian field-based methods. Moment-based models are formed on the basic ideas brought forth in the kinetic theory of gases and provide a useful treatment of multiphase flows. In these models an Eularian formulation of the statistical properties (moments) of the flow is used in order to obtain a treatment of these particle-laden flows. In order to understand how moment-based models are used to describe multiphase flows, it is useful to have an understanding of the fundamentals of kinetic theory, of which moment-based models are build upon. This is the subject of the next chapter.

Chapter 3

Kinetic Theory

Gas flows can be thought of as a collection of particles interacting with each other. In order to properly model these type of situations, Newton's law of motion and classical mechanics can be used in order to model the inter-particle interactions. However, constructing a model based on tracking every single particle in the system, as previously mentioned, becomes prohibitively expensive as the number of particles increase. The kinetic theory of gases, on the other hand, takes the approach of modelling the particles contained in the gas using statistical properties and builds models based on the evolution of theses statistical properties. Classical kinetic theory for monoatomic gases is based upon the following assumptions:

- All matter is composed of discrete particles.
- All particles of a given species are identical.
- Particles are simply points, with no internal structure.
- Particles only exert forces over distances much smaller than the mean-free path.
- Only binary collisions occur between particles, meaning that at most two particles interact in a given collision.
- Quantum effects are neglected.
- Colliding particles are statistically uncorrelated.

Recent advancements in kinetic theory forgoes some of these approximations under certain conditions, but they are currently out of scope for this work.

As classical models of kinetic theory considers gases as a collection of particles, one can see how the techniques applied in kinetic theory can be extended to multiphase flows. This chapter outlines the fundamentals of kinetic theory in order to then apply the principles to a multiphase flow model in Chapter 4.

3.1 An Introduction to the Kinetic Theory of Gases

In a traditional-kinetic theory model, the fluid of interest is assumed to be comprised of discrete particles. These particles are treated in a statistical manner, such that, for a given position in phase space (position and velocity), the number density of particles is given by the distribution function,

$$\mathcal{F} = (x_i, v_i, t) \, . \tag{3.1}$$

The number density of particles in physical space can be obtained by integrating the distribution over the velocity domain,

$$n(x_i, t) = \iiint_{-\infty}^{\infty} \mathcal{F}(x_i, v_i, t) \, \mathrm{d}v_i \, . \tag{3.2}$$

This is what is typically referred to as taking a moment of the distribution function. Taking moments of the distribution creates a relationship between the distribution function and its macroscopic, or observable properties. The moment obtained in Eq. (3.2) is also often referred to as the zeroth-order moment of the distribution. Higher-order moments of the distribution can be obtained in order to relate other macroscopic properties of the flow to the distribution. These higher-order moments are obtained by multiplying the distribution function by weights corresponding to the monomials of the particle velocities and integrating over velocity space. As taking moments of the distribution function is quite common, it becomes useful to define a short-hand angle-bracket notation in order to represent taking the integral over all velocity space,

$$\iiint_{-\infty}^{\infty} w \, \mathcal{F}(x_i, v_i, t) \, \mathrm{d}v_i = \langle \, w \, \mathcal{F} \, \rangle \, . \tag{3.3}$$

Here, w is a velocity dependant weight (typically a monomial). The compact notation, $\langle \cdot \rangle$, indicates integration over all possible velocities. The lowest-order moment, the local number density of a gas, can be obtained by choosing $w = 1$, as presented in Eq. (3.2). As the particle velocity appears zero times in the weight, this is denoted as a zeroth-order moment. Another zeroth-order moment, the mass density, is found by taking $w = m$, where m is the mass of an individual gas particle,

$$\rho = \langle \, m \, \mathcal{F} \, \rangle \, . \tag{3.4}$$

Taking the first-order moment, $w = mv_i$, results in the corresponding momentum density of the particles,

$$\rho \mu_i = \langle \, m v_i \, \mathcal{F} \, \rangle \, . \tag{3.5}$$

The average particle velocity of the distribution can thus be obtained as

$$\mu_i = \frac{\langle \, m v_i \, \mathcal{F} \, \rangle}{\langle \, m \, \mathcal{F} \, \rangle} \, . \tag{3.6}$$

Additionally, it becomes useful to define the random, or deviatoric, velocity of the particles as the difference between the particle's velocity, and the local average velocity of the gas, $c_i = v_i - \mu_i$. The deviatoric velocity can be used to define velocity moments. For example, the moment

$$n\Theta_{ij} = \left\langle c_i c_j \mathcal{F} \right\rangle \,, \tag{3.7}$$

defines the second-order variance-covariance tensor, Θ_{ij}. This symmetric tensor contains the variance of each component of the particle velocity on the diagonal and covariance between components off the diagonal. It is related to the so-called pressure tensor as

$$P_{ij} = \rho\Theta_{ij}. \tag{3.8}$$

This pressure tensor is the negative of the traditional fluid stress tensor and is related to the hydrostatic pressure through the contraction, $p = \frac{1}{3}P_{ii}$. Higher-order moments can also be taken for any given distribution, and while they do have an impact on the distribution function it can prove to be difficult to relate them to physical macroscopic properties that one might observe in the flow. Namely, a third-order moment is used and is referred to as the skewness. This moment related to the skewness is defined as

$$nQ_{ijk} = \left\langle c_i c_j c_k \mathcal{F} \right\rangle \,. \tag{3.9}$$

3.2 Moments Methods

As the distribution of particles, in most useful situations, does not remain constant, a need to model how the distribution evolves over time becomes necessary. This evolution is described by a kinetic equation,

$$\frac{\partial \mathcal{F}}{\partial t} + v_\alpha \frac{\partial \mathcal{F}}{\partial x_\alpha} + \frac{\partial}{\partial v_\alpha}\left(a_\alpha \mathcal{F}\right) = \left(\frac{\delta \mathcal{F}}{\delta t}\right)_{\text{collision}} \,. \tag{3.10}$$

In Eq. (3.10), the first term captures how the distribution changes with time, the second term describes the flux of particles in space, or how the movement of the particles in the system affect the shape of distribution. Next, a_α is the acceleration of the particles due to external forces present on the particles in the distribution. On the right-hand side of Eq. (3.10) is the term representing the collision operator. This collision operator is used to indicate the impact inter-particle collisions have on the distribution. The current flows of interest for this work are assumed dilute and, as such, the impact of collisions on the distribution are ignored,

$$\frac{\delta \mathcal{F}}{\delta t} = 0 \,. \tag{3.11}$$

The kinetic equation described in Eq. (3.10) describes how the distribution function evolves over time. Evaluating this kinetic equation directly can be rather difficult due to the equation being very high-dimensional. In a three-dimensional case, Eq. (3.10) is dependent on three spacial di-

mensions, three velocity dimensions and time, making computation of a direct numerical solution to Eq. (3.10) difficult and expensive to obtain. Rather than trying to evaluate the kinetic equation directly, the use of moments of the distribution can be leveraged in order to model the evolution of the macroscopic properties of the distribution. By taking moments of the kinetic equation, Eq. (3.10), one can obtain a description of how theses moments evolve over time. This gives

$$\left\langle \boldsymbol{\mathcal{W}} \left(\frac{\partial \mathcal{F}}{\partial t} + v_\alpha \frac{\partial \mathcal{F}}{\partial x_\alpha} + \frac{\partial}{\partial v_\alpha} \left(a_\alpha \mathcal{F} \right) \right) \right\rangle = 0 \,, \tag{3.12}$$

$$\left\langle \boldsymbol{\mathcal{W}} \frac{\partial \mathcal{F}}{\partial t} \right\rangle + \left\langle \boldsymbol{\mathcal{W}} v_\alpha \frac{\partial \mathcal{F}}{\partial x_\alpha} \right\rangle + \left\langle \boldsymbol{\mathcal{W}} \frac{\partial}{\partial v_\alpha} \left(a_\alpha \mathcal{F} \right) \right\rangle = 0 \,. \tag{3.13}$$

where the vector $\boldsymbol{\mathcal{W}}$ is used to represent the vector of all the weights that are to be taken of the distribution function in order to build a set of balance laws. Because velocity and time are independent and position and velocity are independent the expression can be simplified into the following balance law form,

$$\frac{\partial}{\partial t} \left\langle \boldsymbol{\mathcal{W}} \mathcal{F} \right\rangle + \frac{\partial}{\partial x_\alpha} \left\langle v_\alpha \boldsymbol{\mathcal{W}} \mathcal{F} \right\rangle + \left\langle \boldsymbol{\mathcal{W}} \frac{\partial}{\partial v_\alpha} \left(a_\alpha \mathcal{F} \right) \right\rangle = 0 \,. \tag{3.14}$$

The acceleration term present in Eq. (3.14) can be expressed as the following using the product rule,

$$\left\langle \frac{\partial}{\partial v_\alpha} \left(a_\alpha \boldsymbol{\mathcal{W}} \mathcal{F} \right) \right\rangle = \left\langle \boldsymbol{\mathcal{W}} \frac{\partial}{\partial v_\alpha} \left(a_\alpha \mathcal{F} \right) \right\rangle + \left\langle a_\alpha \mathcal{F} \frac{\partial}{\partial v_\alpha} \left(\boldsymbol{\mathcal{W}} \right) \right\rangle \,. \tag{3.15}$$

Applying the divergence theorem to the first term of Eq. (3.15), one obtains,

$$\left\langle \frac{\partial}{\partial v_\alpha} \left(a_\alpha \boldsymbol{\mathcal{W}} \mathcal{F} \right) \right\rangle = \iiint_{-\infty}^{\infty} \frac{\partial}{\partial v_\alpha} \left(a_\alpha \boldsymbol{\mathcal{W}} \mathcal{F} \right) \mathrm{d}v_\alpha = \lim_{S \to \infty} \oiint_S \left(a_\alpha \boldsymbol{\mathcal{W}} \mathcal{F} \right) \hat{n}_\alpha \mathrm{d}s \,. \tag{3.16}$$

In its limit, as one evaluates the surface integral of Eq. (3.16), evaluation of $\mathcal{F}$ tends to zero. As such the following holds true

$$\left\langle \frac{\partial}{\partial v_\alpha} \left(a_\alpha \boldsymbol{\mathcal{W}} \mathcal{F} \right) \right\rangle = 0 \,. \tag{3.17}$$

Eq. (3.14) can thus be simplified to

$$\frac{\partial}{\partial t} \left\langle \boldsymbol{\mathcal{W}} \mathcal{F} \right\rangle + \frac{\partial}{\partial x_\alpha} \left\langle v_\alpha \boldsymbol{\mathcal{W}} \mathcal{F} \right\rangle = \left\langle a_\alpha \mathcal{F} \frac{\partial}{\partial v_\alpha} \left(\boldsymbol{\mathcal{W}} \right) \right\rangle \,. \tag{3.18}$$

It becomes useful to present the kinetic equation in its more common balance law form,

$$\frac{\partial}{\partial t} \boldsymbol{U} + \frac{\partial}{\partial x_\alpha} \boldsymbol{F_\alpha} = \boldsymbol{S} \,, \tag{3.19}$$

where $\boldsymbol{U} = \left\langle \boldsymbol{\mathcal{W}} \mathcal{F} \right\rangle$ is the solution vector for the moments of interest and $\boldsymbol{F_\alpha} = \left\langle v_\alpha \boldsymbol{\mathcal{W}} \mathcal{F} \right\rangle$ is the flux dyad corresponding to the conserved moment in $\boldsymbol{U}$. The vector of weights, $\boldsymbol{\mathcal{W}}$ is used to generate the solution vector, $\boldsymbol{U}$. Finally, $\boldsymbol{S}$ is the source term vector resulting from to the forces

present in the system. One can observe that all moments present in the solution vector, $\boldsymbol{U}$ always depend on knowledge of a higher-order moment in the flux term, $\boldsymbol{F}_\alpha$. This dependency makes it difficult to obtain a closed set of PDEs describing the evolution of the distribution over time as the addition of a moment in the solution vector, $\boldsymbol{U}$ always require knowledge of a higher-order moment in the flux term. In order to close the set of PDEs, the form of the distribution function, $\mathcal{F}$, is often assumed. Assuming the form of the distribution means that one can directly evaluate the moments present in the flux term. The process of obtaining a closed set of PDEs are often called moment-closure techniques and are explored in the following sections.

3.3 The Maximum-Entropy Hierarchy

The maximum-entropy hierarchy of moment models, the moment-closure technique used in this work, attempts to close the distribution function by first prescribing the form of the distribution function [15, 19]. By assuming the form of the distribution function the higher-order moments present in the flux term can be obtained as a function of the lower-order moments by directly evaluating the moments of the distribution function. Once the form of the distribution has been assumed and an appropriate set of weights, $\boldsymbol{\mathcal{W}}$, selected, a coupled set of PDEs in closed form can be obtained to describe the evolution of the moments in the system. The maximum-entropy model aims to close the distribution function by selecting a distribution function, $\mathcal{F}$, that is consistent with the known moments, such that the solution vector is recovered

$$\boldsymbol{U} = \langle \boldsymbol{\mathcal{W}} \mathcal{F} \rangle \,, \tag{3.20}$$

and that maximizes entropy. The entropy of a system in the field of kinetic theory takes the form

$$\langle \mathcal{F} \ln \mathcal{F} \rangle \ . \tag{3.21}$$

By this definition it is the negative of the traditional thermodynamic entropy of the system [10, 15, 16]. This is an assumption, that the distribution, $\mathcal{F}$, takes on the maximum-entropy form but it can be argued that given an incomplete knowledge of the system the distribution tends to the maximum-entropy form [19]. In other words, as the only information known from the system is the solution vector, $\boldsymbol{U}$, the distribution function takes a form that is the most likely-state such that it recovers the solution vector, $\boldsymbol{U}$.

This entropy maximization problem can be expressed with the use of Lagrangian multipliers. Eq. (3.21), can be expressed as an unconstrained problem such that the Lagrangian $\boldsymbol{H}$ is expressed as

$$\boldsymbol{H} = \langle \mathcal{F} \ln \mathcal{F} \rangle + \boldsymbol{\lambda}^T \left(\langle \boldsymbol{\mathcal{W}} \mathcal{F} \rangle - \boldsymbol{U} \right) \,, \tag{3.22}$$

where $\boldsymbol{\lambda}$ is the vector of Lagrangian multipliers corresponding to the constraints in Eq. (3.20). This function is maximal when

$$\frac{\partial \boldsymbol{H}}{\partial \mathcal{F}} = 0 \,, \tag{3.23}$$

such that,

$$\frac{\partial \boldsymbol{H}}{\partial \mathcal{F}} = \left\langle \ln \mathcal{F} - \frac{\mathcal{F}}{\mathcal{F}} \right\rangle + \boldsymbol{\lambda}^T \left\langle \boldsymbol{\mathcal{W}} \right\rangle \ . \tag{3.24}$$

Eq. (3.24) can then be expressed in the form,

$$0 = \left\langle \ln \mathcal{F} - 1 + \boldsymbol{\lambda}^T \boldsymbol{\mathcal{W}} \right\rangle \ , \tag{3.25}$$

where an expression for $\mathcal{F}$ that maximizes entropy can be obtained,

$$\mathcal{F} = \exp \left[1 - \boldsymbol{\lambda}^T \boldsymbol{\mathcal{W}} \right] . \tag{3.26}$$

For this maximum-entropy moment closure technique the Lagrange multipliers are often expressed as a finite number of free parameters, $\boldsymbol{\alpha}$, often called the closure coefficients,

$$\mathcal{F} = \exp \left[\boldsymbol{\alpha}^T \boldsymbol{\mathcal{W}} \right] . \tag{3.27}$$

The number of free parameters, $\boldsymbol{\alpha}$, must therefore be equal to the size of the solution vector, $\boldsymbol{U}$, and by extension the vector of generating weights, $\boldsymbol{\mathcal{W}}$. Selection of the free parameters such that they respect the solution vector, Eq. (3.20), Eq. (3.21), results in a maximum-entropy model for the distribution function [15].

3.4 The Hyperbolicity of The Maximum-Entropy Model

It is possible that the resulting set of PDEs obtained in Eq. (3.19) can result in a set of ill-posed non-hyperbolic PDEs. For this reason, a certain amount of care needs to be put into the selection of the distribution function and the selected vector of weights, $\boldsymbol{\mathcal{W}}$ in order to guarantee a set of hyperbolic PDEs. Therefore, it is important to show that for the given system, Eq. (3.19), the set of PDEs are hyperbolic. With adequate selection of the free parameters, $\boldsymbol{\alpha}$ in Eq. (3.27) and of the generating weights, $\boldsymbol{\mathcal{W}}$ it can be shown that the hyperbolicity of the system is guaranteed. To begin, one can observe that for any given set of real vectors, $\boldsymbol{\mathcal{W}}$, and the selection of any real closure coefficients, $\boldsymbol{\alpha}$, the distribution function always admits a positive distribution due to the assumed form of the distribution containing an exponential. Furthermore, the hyperbolicity of the moment equation can be confirmed by firstly defining the density and flux potentials as

$$h(\boldsymbol{\alpha}) = \langle \boldsymbol{\mathcal{F}} \rangle = \left\langle e^{\boldsymbol{\alpha}^T \boldsymbol{\mathcal{W}}} \right\rangle \ , \tag{3.28}$$

$$f_i(\boldsymbol{\alpha}) = \langle v_i \boldsymbol{\mathcal{F}} \rangle = \left\langle v_i e^{\boldsymbol{\alpha}^T \boldsymbol{\mathcal{W}}} \right\rangle \ . \tag{3.29}$$

The derivative of the density and flux potentials with respect to the closure coefficients, $\boldsymbol{\alpha}$, can then be taken in order to obtain the solution vector, $\boldsymbol{U}$, and flux dyad, $\boldsymbol{F}_i$, that are present in the

balance-law,

$$\boldsymbol{U} = \frac{\partial h(\boldsymbol{\alpha})}{\partial \boldsymbol{\alpha}} = \left\langle \boldsymbol{\curlywedge} e^{\boldsymbol{\alpha}^T \boldsymbol{\curlywedge}} \right\rangle , \tag{3.30}$$

$$\boldsymbol{F}_i = \frac{\partial f_i(\boldsymbol{\alpha})}{\partial \boldsymbol{\alpha}} = \left\langle v_i \boldsymbol{\curlywedge} e^{\boldsymbol{\alpha}^T \boldsymbol{\curlywedge}} \right\rangle . \tag{3.31}$$

The balance law, Eq. (3.19), can then be expressed in terms of the partial derivatives with respect to the free parameters such that the balance law takes the form

$$\frac{\partial}{\partial t} \frac{\partial h(\boldsymbol{\alpha})}{\partial \boldsymbol{\alpha}} + \frac{\partial}{\partial x_\alpha} \frac{\partial f_i(\boldsymbol{\alpha})}{\partial \boldsymbol{\alpha}} = \boldsymbol{S} . \tag{3.32}$$

Both the solution vector and the flux vector can be differentiated by the closure coefficients again in order to obtain the flux Jacobian of the balance law in an alternative form

$$h(\boldsymbol{\alpha})_{,\boldsymbol{\alpha},\boldsymbol{\alpha}} = \frac{\partial^2 h(\boldsymbol{\alpha})}{\partial \boldsymbol{\alpha} \partial \boldsymbol{\alpha}} = \left\langle \boldsymbol{\curlywedge} \boldsymbol{\curlywedge}^T e^{\boldsymbol{\alpha}^T \boldsymbol{\curlywedge}} \right\rangle , \tag{3.33}$$

$$f_i(\boldsymbol{\alpha})_{,\boldsymbol{\alpha},\boldsymbol{\alpha}} = \frac{\partial^2 f_i(\boldsymbol{\alpha})}{\partial \boldsymbol{\alpha} \partial \boldsymbol{\alpha}} = \left\langle v_i \boldsymbol{\curlywedge} \boldsymbol{\curlywedge}^T e^{\boldsymbol{\alpha}^T \boldsymbol{\curlywedge}} \right\rangle , \tag{3.34}$$

where one can then define the flux Jacobian of the balance law as

$$\frac{\partial \boldsymbol{F}}{\partial \boldsymbol{U}} = \left(\frac{\partial \boldsymbol{U}}{\partial \alpha} \right)^{-1} \frac{\partial \boldsymbol{F}}{\partial \boldsymbol{\alpha}} = h(\boldsymbol{\alpha})^{-1}_{,\boldsymbol{\alpha},\boldsymbol{\alpha}} f_i(\boldsymbol{\alpha})_{,\boldsymbol{\alpha},\boldsymbol{\alpha}} . \tag{3.35}$$

The balance law can now be expressed in terms of the second derivatives of the closure coefficients, such that the original balance equation,

$$\frac{\partial}{\partial t} \boldsymbol{U} + \frac{\partial}{\partial x_\alpha} \boldsymbol{F}_{\boldsymbol{\alpha}} = \boldsymbol{S} , \tag{3.36}$$

can be written as

$$\frac{\partial^2 h(\boldsymbol{\alpha})}{\partial \boldsymbol{\alpha} \partial \boldsymbol{\alpha}} \frac{\partial \boldsymbol{\alpha}}{\partial t} + \frac{\partial^2 f_i(\boldsymbol{\alpha})}{\partial \boldsymbol{\alpha} \partial \boldsymbol{\alpha}} \frac{\partial \boldsymbol{\alpha}}{\partial x_\alpha} = \boldsymbol{S} , \tag{3.37}$$

$$h(\boldsymbol{\alpha})_{,\boldsymbol{\alpha},\boldsymbol{\alpha}} \frac{\partial \boldsymbol{\alpha}}{\partial t} + f_i(\boldsymbol{\alpha})_{,\boldsymbol{\alpha},\boldsymbol{\alpha}} \frac{\partial \boldsymbol{\alpha}}{\partial x_\alpha} = \boldsymbol{S} . \tag{3.38}$$

Eq. (3.38) describes the variation of the free parameters, $\boldsymbol{\alpha}$, for a maximum-entropy distribution. In order to guaranteed a hyperbolic system, one has to prove that the flux Jacobian, only has real eigenvalues and is diagonalizable. It follows that the flux Jacobian of the system, only has real eigenvalues and is diagonalizable if and only if $h(\boldsymbol{\alpha})_{,\boldsymbol{\alpha},\boldsymbol{\alpha}}$ is non-singular and symmetric. Analyzing the density potential,

$$h(\boldsymbol{\alpha})_{,\boldsymbol{\alpha},\boldsymbol{\alpha}} = \frac{\partial^2 h(\boldsymbol{\alpha})}{\partial \boldsymbol{\alpha} \partial \boldsymbol{\alpha}} = \left\langle \boldsymbol{\curlywedge} \boldsymbol{\curlywedge}^T \mathcal{F} \right\rangle , \tag{3.39}$$

one can notice that for any given vector, $\boldsymbol{\mathcal{W}}$, the resulting product $\boldsymbol{\mathcal{W}}\boldsymbol{\mathcal{W}}^T$ is always symmetric and semi-positive definite. Such that it can be shown that for any given vector, $\boldsymbol{w}$,

$$\boldsymbol{w}^T h(\boldsymbol{\alpha})_{,\boldsymbol{\alpha},\boldsymbol{\alpha}} \boldsymbol{w} = \left\langle \boldsymbol{w}^T \boldsymbol{\mathcal{W}} \boldsymbol{\mathcal{W}}^T \mathcal{F} \boldsymbol{w} \right\rangle = \left\langle \left(\boldsymbol{w}^T \boldsymbol{\mathcal{W}} \right)^2 \mathcal{F} \right\rangle \geq 0 \,, \tag{3.40}$$

as $\mathcal{F}$ has to admit positive real values and $\boldsymbol{w}$ is assumed to be a non-zero vector such that the expression $\left(\boldsymbol{w}^T \boldsymbol{\mathcal{W}}\right)^2$ will always be positive, one can guaranteed that $h(\boldsymbol{\alpha})_{,\boldsymbol{\alpha},\boldsymbol{\alpha}}$ is a strictly convex function and is positive-definite.

3.5 A Simple Maximum Entropy Model

The lowest-order member of the maximum-entropy hierarchy is obtained by choosing a vector of generating weights, $\boldsymbol{\mathcal{W}}_5 = [m, mv_i, \frac{1}{2} mv_i v_i]^{\mathrm{T}}$. This gives an assumed form of the distribution function given by

$$\mathcal{F}_5 = n \left(\frac{\rho}{2\pi p} \right)^{\frac{3}{2}} \exp \left(-\frac{\rho}{2p} c_i c_i \right) \,, \tag{3.41}$$

which is the Maxwell-Boltzmann distribution that describes a gas in local thermodynamic equilibrium, and leads to the familiar Euler equations for a compressible monatomic gas,

$$\frac{\partial \rho}{\partial t} + \frac{\partial}{\partial x_k} \rho \mu_k = 0 \,, \tag{3.42}$$

$$\frac{\partial}{\partial t} \rho \mu_i + \frac{\partial}{\partial x_k} \left(\rho \mu_i \mu_k \right) = 0 \,. \tag{3.43}$$

The next member of the maximum-entropy family of closures uses the ten moments that correspond to velocity weights, $\boldsymbol{\mathcal{W}}_{10} = [m, mv_i, mv_i v_j]^{\mathrm{T}}$. This leads to a distribution function given by

$$\mathcal{F}_{10} = \mathcal{G} = \frac{n}{(2\pi)^{\frac{3}{2}} \left(\det \Theta_{ij} \right)^{\frac{1}{2}}} \exp \left(-\frac{1}{2} \Theta_{ij}^{-1} c_i c_j \right) \,. \tag{3.44}$$

This so-called Gaussian distribution resembles the Maxwell-Boltzmann distribution, but has a different velocity variance in different directions. A relationship from the moment variables in Eq. (3.44), to the closure coefficients, α can be derived such that,

$$\boldsymbol{\alpha} = \left[\log \left(\frac{\rho}{\left(det \Theta_{ij} \right)^{1/2}} \right) - \frac{1}{2} \Theta_{ij}^{-1} \mu_i \mu_j, \; \Theta_{ij}^{-1} \mu_i, \; -\frac{1}{2} \Theta_{ij}^{-1} \right]^T \,. \tag{3.45}$$

In the absence of acceleration fields, it leads to a collection of ten first-order hyperbolic balance

laws,

$$\frac{\partial \rho}{\partial t} + \frac{\partial}{\partial x_k} \rho \mu_k = 0 \,, \tag{3.46}$$

$$\frac{\partial}{\partial t} \rho \mu_i + \frac{\partial}{\partial x_k} \left(\rho \mu_i \mu_k + P_{ik} \right) = 0 \,, \tag{3.47}$$

$$\frac{\partial}{\partial t} \left(\rho \mu_i \mu_k + P_{ik} \right) + \frac{\partial}{\partial x_k} \left(\rho \mu_i \mu_j \mu_k + \mu_i P_{jk} + \mu_j P_{ik} + \mu_k P_{ij} \right) = \Delta(P_{ij}) \,. \tag{3.48}$$

Here, $\Delta(P_{ij})$ describes how inter-particle collisions attenuate anisotropy in the pressure tensor. This term depends of the particular collision operator chosen. This closure provides a first-order hyperbolic treatment for viscous compressible gases. It obtains its closure because the heat transfer is zero through the choice of the distribution function. However, this model has been used to successfully model many viscous flows in situations when heat-transfer can be neglected [2, 13, 16, 18, 27] This model has also previously been applied to the prediction of monodisperse flows with good results [30]. It is this Gaussian model that forms the basis of the treatments for polydisperse multiphase proposed in the present work. Having the distribution function expressed as lower-order moments proves to be vital as this is what is used to obtain the higher-order flux term in Eq. (3.19).

Chapter 4

A Polydisperse Gaussian Model

This current work is based on a treatment of multiphase flows based on a kinetic-theory approach. There exist many ways to treat polydisperse flows with kinetic theory. One can notice that the fundamental assumptions of kinetic theory, that a gas is composed of small particles and models are constructed based on tracking statistical moments of these particles and not every single particle in the flow, lends itself nicely for applications of polydisperse mulitphase flows. Moment-based methods also have other nice properties, such as being able to be represented in a balance-law form. Having the equations derived in their balance-law form enables the simple implementation into a Godunov-type or discontinuous-Galerkin scheme for computational simulations. There are many ways multiphase polydisperse flows can be treated with a kinetic theory approach and are explored in the following sections.

4.0.1 Single-Velocity Model

In this single velocity model, the solution vector contains the mass and momentum density,

$$\boldsymbol{U} = [\rho,\ \rho\mu_i]^T\ . \tag{4.1}$$

In this simple model, the distribution function is selected such that all the particles at a given location have the same velocity. While the single-velocity model might be useful in modelling multiphase flows for very low Stokes numbers, such that particles in the flow have a tightly coupled velocity, in many situations where drag plays a less significant role in the velocity of the particles, a simple single-velocity model is insufficient. In the case of polydisperse flows where these flows contain a wide range of particle sizes, and by extension a wide range of particle velocities due to the effects of drag, the single velocity model is unable to capture the range of velocities present is such flows. Most notability, the use of the single velocity model in problems containing streams of particles crossing result in significant mathematical artifacts [28] .

4.0.2 Quadrature-Based Methods

Quadrature-based moment-methods (QBM) have been developed in order to overcome the limitations in the single velocity-models. The main issue with the single velocity model is that it

is unable to admit, at a given point in space a varying velocities of particles. While the single-velocity model admits various particle velocities at different locations in space, at a given point in space all particles must have the same velocity. It can be augured that this the main cause of mathematical artifacts and modelling inaccuracies present in certain problems such as particle stream crossing. In a QBM treatment for polydisperse multiphase flows, the model relies on the principle of "binning". Such that for a given position in space, the particles can admit a finite set of velocities [17, 6]. While these models have been shown to be successful they still remain difficult to implement. As QBM rely on this principle of "binning" for the particles velocities an algorithm must be implemented in order to numerically divide the distribution function in to the velocity bins.

4.0.3 Gaussian-based Maximum-Entropy Models

Gaussian moment-methods, and the method used in the implementation of the PGM rely on an extension of the initial distribution function derived from kinetic theory. In order to extend the traditional kinetic theory model to polydisperse flows, one must first redefine the original distribution function. The standard distribution in a traditional kinetic theory model defines the distribution as, $\mathcal{F}(x_i, v_i, t)$ where $\mathcal{F}$, is the number of particles found with a certain position, x_i, with a chosen velocity, v_i, and at a given time, t. This distribution can then be extended to any number of distinguishing internal variables that one might use in order to differentiate the particles in the system,

$$\mathcal{F} = \mathcal{F}(x_i, v_i, \zeta_{\check{i}}, t)\,, \tag{4.2}$$

such that, ζ, is a variable representing some property of the studied particles and the index, $\check{i}$ represents the internal index of the studied variable. These internal variables can take any physical properties of the particles that might be of interest such as size, temperature, or electric charge. In this new distribution, the number density is obtained for particles given a position in phase-space and a value for the selected internal variables. Eq. (4.2), can be interpreted as asking, "at any given time, t how many particles in the current system have a given position, velocity, and set value of internal variables?". The evolution of the distribution can then be described with a kinetic equation,

$$\frac{\partial \mathcal{F}}{\partial t} + v_\alpha \frac{\partial \mathcal{F}}{\partial x_\alpha} + \frac{\partial}{\partial v_\alpha}\left(a_\alpha \mathcal{F}\right) + \sum_{\check{i}=0} \frac{\partial}{\partial \zeta_{\check{i}}}\left(\Upsilon_{\check{i}} \mathcal{F}\right) = \left(\frac{\delta \mathcal{F}}{\delta t}\right)_{\text{collision}}. \tag{4.3}$$

Eq. (4.3), is an extension of the previous kinetic equation and represents the change of the new distribution, $\mathcal{F}$ over time. Eq. (4.3), still captures the effect the flux of particles in the system has on the shape of the distribution, and a_α is still the acceleration of the particles due to external forces acting on the particles but now there is the added term corresponding to rate of change of the particles differentiating variables. The additional term, $\Upsilon_{\check{i}}$ is the rate of change of the $\check{i}$th internal variable. On the right-hand side of Eq. (4.3) is still the term representing the collision operator. As previously mentioned the impact collisions have on the distribution function are not

considered in the scope of this work.

Defining the distribution with internal properties is critical as the flows studied in this work are polydisperse and being able to capture particle size into the kinetic equation is critical to the development of a polydisperse multiphase kinetic model.

4.1 Moments of a Multivariate Gaussian Moment Model

In Gaussian moment-models, the distribution function is altered in order to capture other information that might be important in the studied flows. Due to this alteration of the distribution function, the moments obtained from the distribution might be different than those in a traditional gas-kinetic model. In order to relate the distribution function to the macroscopic properties of the flow, moments of $\mathcal{F}$ can be taken similarly to those in a traditional kinetic model. The moments that are taken not only cover velocity space but also over the internal variables of the distribution, such that the notation of a moment for a given weight, w is as follows

$$\langle w\mathcal{F} \rangle = \iiint_{\infty} \cdots \int w\mathcal{F} \, \mathrm{d}\zeta_{\check{i}} \, \mathrm{d}v_i \, . \tag{4.4}$$

Again the number density and average velocity of the distribution can be obtained by selecting a weight of $w = 1$ and $w = v_i$ respectively,

$$n(x_i, t) = \langle \mathcal{F} \rangle \, , \tag{4.5}$$

$$n\mu_i = \langle v_i \mathcal{F} \rangle \, . \tag{4.6}$$

In addition to the moments defined above, the distinguishing variables can also be used as moment weights. For example, the average value of a distinguishing variable, $\bar{\zeta}_{\check{i}}$, can be found as

$$n\bar{\zeta}_{\check{i}} = \left\langle \zeta_{\check{i}} \mathcal{F} \right\rangle \, . \tag{4.7}$$

This allows the deviatoric velocity, c_i, to be extended with the deviations of other variables from their average,

$$c_{\tilde{i}} = \left[v_x - \mu_x, \; v_y - \mu_y, \; v_z - \mu_z, \; \zeta_0 - \bar{\zeta}_0, \; \zeta_1 - \bar{\zeta}_1, \; \zeta_2 - \bar{\zeta}_2, \; \dots \right]^{\mathrm{T}} \, , \tag{4.8}$$

where indices decorated with a tilde, $c_{\tilde{i}}$, indicate an expanded index comprising the traditional spacial directions and added distinguishing variables[1]. This allows an expanded variance-covariance tensor to be defined as

$$n\Psi_{\tilde{i}\tilde{j}} = n \begin{bmatrix} \Theta_{ij} & \Psi_{i\check{j}} \\ \Psi_{j\check{i}} & \Psi_{\check{i}\check{j}} \end{bmatrix} = \left\langle c_{\tilde{i}} c_{\tilde{j}} \mathcal{F} \right\rangle \, . \tag{4.9}$$

The off-diagonal entries, $\Psi_{i\check{j}}$, contain the covariances between components of the particle velocity and particular distinguishing variables, while $\Psi_{\check{i}\check{j}}$ contains variances and covariances between

[1] It should be noted that the Einstein summation convention is also applied to indices decorated with tildes.

the distinguishing variables themselves. Much like the traditional kinetic model, higher-order moments of the new distribution function can be taken. These moments would result in higher-order tensors such as the skewness that would be related to not only the skewness of the particle velocity but the their relationship to the selected internal variables of the distribution. By taking moments of the kinetic equation, Eq. (4.3), Maxwell's equation of change is obtained for a distribution function with any number of internal distinguishing variables,

$$\frac{\partial}{\partial t}\left\langle \boldsymbol{\mathcal{W}}\mathcal{F}\right\rangle + \frac{\partial}{\partial x_\alpha}\left\langle v_\alpha \boldsymbol{\mathcal{W}}\mathcal{F}\right\rangle = \left\langle a_\alpha \mathcal{F}\frac{\partial}{\partial v_\alpha}\boldsymbol{\mathcal{W}}\right\rangle - \sum_{\check{i}=0}\left\langle \frac{\partial}{\partial \zeta_{\check{i}}}\left(\boldsymbol{\mathcal{W}}\Upsilon_{\check{i}}\mathcal{F}\right)\right\rangle + \sum_{\check{i}=0}\left\langle \Upsilon_{\check{i}}\mathcal{F}\frac{\partial}{\partial \zeta_{\check{i}}}\boldsymbol{\mathcal{W}}\right\rangle . \tag{4.10}$$

Eq. (4.10) provides the model with the evolution of the macroscopic properties of the distribution. One should note that, unlike in Eq. (3.15), the second-last term on the right-hand side of Eq. (4.10) is not necessarily zero, if the domain of one or more of the distinguishing variables is not $(-\infty, \infty)$. Practically, it is more useful to model a set of moments rather than a single moment and much like previously shown, the kinetic equation can also be expressed in a simplified balance-law form,

$$\frac{\partial}{\partial t}\boldsymbol{U} + \frac{\partial}{\partial x_\alpha}\boldsymbol{F_\alpha} = \boldsymbol{S} . \tag{4.11}$$

The contents of the conserved vector of moments, $\boldsymbol{U}$, flux dyad, $\boldsymbol{F_\alpha}$, and source term, $\boldsymbol{S}$, are obviously going to be different than the ones shown in the previous, traditional gas-kinetic model and so are the selected vector of weights, $\boldsymbol{\mathcal{W}}$, but their representation in the balance equation remains the same. The inclusion of distinguishing variables, $\zeta_{\check{i}}$, enables the kinetic model to capture polydisperse flows, as having the internal variable related to the particles size means that the distribution function is able to capture how moments related to the size of the particles in the flow evolves in time. Additionally, moments that are obtained from the Gaussian model can provide useful statistical information not normally captured in other models such as the evolution over time of the covariance between a set of two internal distinguishing variables.

4.2 Moments of a Polydisperse Gaussian Distribution

This section outlines the method of which one can use to obtain moments of the previous PGM model using diameter-based statistics in addition to the new surface-based PGM.

4.2.1 Log-Normal Diameter Based Statistics

In the previous PGM, [5], the natural logarithm of the particle diameter was selected as the internal variable of interest for the PGM. Thus, the distribution function had the form,

$$\mathcal{F}_D = \mathcal{F}(x_i, v_i, ln(d), t) . \tag{4.12}$$

This gives a kinetic description for a polydisperse flow, as information about the particles size is captured into the distribution function [5]. The natural logarithm of the particle diameter was originally selected as the internal variable as it was reasoned that experimental data for aerosol particle diameters often displays a log-normal distribution [5, 12], thus capturing the log-normal distribution into the distribution function was a logical choice. The previous PGM was constructed using the following set of weights,

$$\boldsymbol{\mathcal{W}}_D = \left[1,\ v_i,\ v_i v_j,\ \ln(d),\ v_i \ln(d),\ \ln(d)^2\right]^T \ . \tag{4.13}$$

Applying the principles of maximum entropy moment-closure techniques the distribution function can be obtained in closed form as a function of all the lower-order moments. Theses moments are outlined as follows. The number density of the particles is given by

$$n = \langle \mathcal{F}_D \rangle \ , \tag{4.14}$$

whereas the particles average velocity and log-average diameter are given by,

$$n\mu_i = \langle v_i \mathcal{F}_D \rangle \ , \tag{4.15}$$

$$n\mu_d = \langle \ln d \mathcal{F}_D \rangle \ . \tag{4.16}$$

The variance tensor for the particles velocities and their covariance relationship to the log-normal average diameter is given by,

$$n\Theta_{ij} = \left\langle (v_i - \mu_i)(v_j - \mu_j)\mathcal{F}_D \right\rangle \ , \tag{4.17}$$

$$n\Psi_{id} = \langle (v_i - \mu_i)(\ln d - \mu_d)\mathcal{F}_D \rangle \ , \tag{4.18}$$

$$n\Psi_{dd} = \left\langle (\ln d - \mu_d)^2 \mathcal{F}_D \right\rangle \ . \tag{4.19}$$

With the moments of $\mathcal{F}_D$ properly defined the assumed from of the distribution function can be obtained in order to close the set of obtained PDEs as

$$\mathcal{F}_D = \frac{n}{(2\pi)^{\frac{3+N}{2}} (\det \Psi_{\tilde{i}\tilde{j}})^{\frac{1}{2}}} \exp\left[-\frac{1}{2}\Psi^{-1}_{\tilde{i}\tilde{j}} \tilde{c}_i \tilde{c}_j\right] \ . \tag{4.20}$$

In this form, the diameter-based PGM the $\tilde{c}_i$ vector is expressed as the following for a three-dimensional case

$$\tilde{c}_i = \begin{bmatrix} v_x - \mu_x \\ v_y - \mu_y \\ v_z - \mu_z \\ \ln d - \mu_d \end{bmatrix} , \tag{4.21}$$

and the $\Psi_{\tilde{i}\tilde{j}}$ tensor takes on the form

$$\Psi_{\tilde{i}\tilde{j}} = \begin{bmatrix} \Theta_{xx} & \Theta_{xy} & \Theta_{xz} & \Psi_{zd} \\ \Theta_{xy} & \Theta_{yy} & \Theta_{yz} & \Psi_{zd} \\ \Theta_{xz} & \Theta_{zy} & \Theta_{zz} & \Psi_{zd} \\ \Psi_{xd} & \Psi_{zd} & \Psi_{zd} & \Psi_{dd} \end{bmatrix} . \tag{4.22}$$

While the previous PGM showed very promising results, it failed to capture the exact steady-state solution of particles settling in a flow [5] . In order to more closely follow the results obtained by directly solving for the kinetic equation the relaxation parameter in the source term had to be tuned to the problem. To reduce this issue the particle surface can instead be used as the internal variable of choice. The reasoning is that, particles settling in a Stokes flow reach a steady-state distribution depending on the particles surface area due to drag under Stokes flow being proportional to the diameter squared. Thus, capturing the particle surface in the distribution function enables the distribution to recover the steady-state solution. This recovery of the steady-state solution is shown in further detail in Section 4.4. The distribution, $\mathcal{F}$, for the PGM presented in this work becomes a function of position in phase-space and the particles surface area,

$$\mathcal{F} = \mathcal{F}(x_i, v_i, s, t) . \tag{4.23}$$

In Eq. (4.23), as the particles surface area can only take on strictly positive values moments of the distribution function are taken as,

$$\langle w\mathcal{F} \rangle = \iiint_{\infty} \int_{0}^{\infty} w\mathcal{F} \, \mathrm{d}s \, \mathrm{d}v_i . \tag{4.24}$$

4.2.2 Surface-Based Statistics

The moments for the surface-weighted PGM are defined as the following for the temainder of this work. As previously shown the distribution takes on the following form,

$$\mathcal{F} = \mathcal{F}(x_i, v_i, s, t) . \tag{4.25}$$

The moments are similar to those previously derived in Section 4.2.1. For the construction of the surface-based PGM the corresponding moments are such that the number density is given by,

$$n = \langle \mathcal{F} \rangle \ . \tag{4.26}$$

The average particle velocity and surface are given by the two moments equations,

$$n\mu_i = \langle v_i \, \mathcal{F} \rangle , \tag{4.27}$$

$$n\sigma = \langle s \, \mathcal{F} \rangle . \tag{4.28}$$

Where, s corresponds to the particles particular surface area and the average surface is given by σ. For the surface-based PGM the particles random velocity and random surface area are defined respectively as the difference between their particular variable and their local average,

$$c_i = v_i - \mu_i \,, \tag{4.29}$$

$$c_s = s - \sigma \,. \tag{4.30}$$

The variance-covariance tensor corresponding to the particle velocity, takes the following form,

$$n\Theta_{ij} = \left\langle (v_i - \mu_i)(v_j - \mu_j)\mathcal{F} \right\rangle \,, \tag{4.31}$$

$$n\Theta_{ij} = \left\langle c_i c_j \mathcal{F} \right\rangle \,. \tag{4.32}$$

In addition to the variance-covariance tensor, a covariance vector relating a particle's velocity with its respective surface is defined as

$$n\Psi_{is} = \langle c_i c_s \mathcal{F} \rangle \,. \tag{4.33}$$

Finally, a scalar representing the variance of the particles surface area in the system is given by the following moment,

$$n\Psi_{ss} = \left\langle c_s^2 \mathcal{F} \right\rangle \,. \tag{4.34}$$

As previously mentioned, in addition to the definition of the second-order moments of the PGM, due to the presence of a high-order moment in the flux term, it is also necessary to define a third-order moment in order to obtain the full set of PDEs. The third-order moment, or often called the skewness in the field of statics is defined as Q_{ijk}. The skewness of the particle velocity is thus defined as the following,

$$nQ_{ijk} = \left\langle c_i c_j c_k \mathcal{F} \right\rangle \,. \tag{4.35}$$

In addition to the flux term for the particle velocity, a moment for the flux of covariance of the particle velocity with respect to its surface and a moment for the flux with the variance of particle velocity must also be defined,

$$nQ_{ijs} = \left\langle c_i c_j c_s \mathcal{F} \right\rangle \,, \tag{4.36}$$

$$nQ_{iss} = \left\langle c_i c_s^2 \mathcal{F} \right\rangle \,. \tag{4.37}$$

While it might be difficult to relate the multivariate skewness, namely Q_{ijs} and Q_{iss} to physical and observable properties of the flow, such as the average velocity or pressure tensor of the fluid, they are nonetheless critical to discribe the evolution of the lower-order moments. With all the moments properly defined one can begin to construct the set of balance laws for the PGM.

4.2.3 The PGM in Balance-Law Form

Given the following set of weights, $\boldsymbol{\mathcal{W}} = \left[1, v_i, v_i v_j, s, v_i s, s^2\right]$, the PGM can be presented in its balance law form as

$$\frac{\partial n}{\partial t} + \frac{\partial}{\partial x_\alpha} n\mu_\alpha = S^{(1)}, \tag{4.38}$$

$$\frac{\partial}{\partial t} n\mu_i + \frac{\partial}{\partial x_\alpha} n(\Theta_{i\alpha} + \mu_i\mu_\alpha) = S_i^{(2)}, \tag{4.39}$$

$$\frac{\partial}{\partial t} n\left(\Theta_{ij} + \mu_i\mu_j\right) + \frac{\partial}{\partial x_\alpha} n\left(Q_{ij\alpha} + \mu_i\Theta_{j\alpha} + \mu_j\Theta_{i\alpha} + \mu_\alpha\Theta_{ij} + \mu_i\mu_j\mu_\alpha\right) = S_{ij}^{(3)}, \tag{4.40}$$

$$\frac{\partial}{\partial t} n\sigma + \frac{\partial}{\partial x_\alpha} n\left(\Psi_{\alpha s} + \mu_\alpha\sigma\right) = S_s^{(4)}, \tag{4.41}$$

$$\frac{\partial}{\partial t} n(\Psi_{is} + \mu_i\sigma) + \frac{\partial}{\partial x_\alpha} n\left(Q_{i\alpha s} + \mu_i\Psi_{\alpha s} + \mu_\alpha\Psi_{is} + \sigma\Theta_{i\alpha} + \mu_i\mu_\alpha\sigma\right) = S_{is}^{(5)}, \tag{4.42}$$

$$\frac{\partial}{\partial t} n(\Psi_{ss} + \sigma^2) + \frac{\partial}{\partial x_\alpha} n\left(Q_{iss} + 2\sigma\Psi_{\alpha s} + \mu_\alpha\Psi_{ss} + \mu_\alpha\sigma^2\right) = S_{ss}^{(6)}. \tag{4.43}$$

In this form, the source term subscripts correspond to the sources respective moment weights. Whereas the superscript is used to indicate the row of the source term in the solution vector $\boldsymbol{U}$. In this balance-law form, one can explore the information obtained in the solution vector,

$$\boldsymbol{U} = n\begin{bmatrix} 1 \\ \mu_i \\ \Theta_{ij} + \mu_i\mu_j \\ \sigma \\ \Psi_{is} + \mu_i\sigma \\ \Psi_{ss} + \sigma^2 \end{bmatrix}. \tag{4.44}$$

Starting from the top of the solution vector, $\boldsymbol{U}$, the first equation obtained is pretty self explanatory and provides a description on how the number density of the particles in the system changes with time. Next, μ_i is a vector that captures the average velocity of the particles at a location. The tensor, Θ_{ij}, is the velocity variance tensor indicating the spread of particle velocity. As shown in Eq. (4.44), not only does this tensor capture the variance of particle velocities in a given direction, *e.g.* Θ_{xx}, but also captures the covariance between two different velocities, Θ_{xy}. This variance provides information as to the spread of velocities from the mean velocity of the distribution in a given direction. A large variance in the x direction, Θ_{xx}, would indicate that the particles velocities are rather spread out from the average, μ_x. A smaller Θ_{xx} direction variance would indicate that the particle velocities are more tightly coupled to the their local average, μ_x. In the cross-term of velocities for instance Θ_{xy}, is the covariance relationship between the particles x and y velocities. Zero velocity covariance would indicate that there is no relationship between the particles x velocity and y velocity. A positive covariance in Θ_{xy} would indicate a positive coupling between the two velocities, such that particles that have a large positive x velocity are

also more likely to have a large positive y velocity. A negative covariance, Θ_{xy} would indicate an inverse of the coupling relationship, such that a large positive velocity in a given direction more-likely relates to a large negative velocity in the other. The scalar, σ, captures the evolution of the average particle surface area over time. This is critical to the development of a polydisperse model, as information relating to the size of the particles can be obtained as a function of time and space. The next term, Ψ_{is}, is a vector of the covariance between the particle velocity and size for each spacial dimension. This term is rather interesting as it contains information that would typically not be captured in traditional multiphase models. This vector provides information as to the coupling between the particle velocity and surface area, *i.e.* particle size. A large positive covariance indicates a strong correlation between the particle size and velocity, such that larger particles are more likely to have a larger velocity and smaller particles are more likely to be travelling at a slower velocity. This information is very useful when developing an understanding as to the movement of particles in a polydisperse multiphase flow as the covariance term provides information as to how the range of particle size in the system can affect the outcome of the flow. Finally, the scalar, Ψ_{ss}, is the variance of the particle size such that the PGM also captures the rate of change of the variance of particle surface area at a given location. Again, much like the velocity variance, a large variance of the surface would indicate that the particles at a given location admit a wide range of sizes spread apart from its average, σ. A smaller variance would mean that the particles are very close to the average particle size, σ.

4.2.4 The PGM in Closed Form

The maximum entropy form of the distribution function, Eq. (3.27) as previously shown takes the form of exponential raised to the power of a polynomial of the closure coefficients, $\boldsymbol{\alpha}$. It can be shown that the maximum entropy form of the distribution can be written in the form of a multivariate Gaussian distribution,

$$\mathcal{F} = \exp\left[-\frac{1}{2}\boldsymbol{c}^T\boldsymbol{M}^{-1}\boldsymbol{c} + k\right], \tag{4.45}$$

with

$$\boldsymbol{M} = \begin{bmatrix} p_{ij} & q_{is} \\ q_{js} & r_{ss} \end{bmatrix} \quad \boldsymbol{c} = \begin{bmatrix} v_i - \hat{u}_i \\ s - \hat{s} \end{bmatrix}. \tag{4.46}$$

For the distribution function presented in Eq. (4.45), a relation can be build between the variables in the multivariate Gaussian, $p_{ij}, q_{is}, r_{ss}, \hat{u}_i, \hat{s}, k$ and the maximum-entropy vector, $\boldsymbol{\alpha}$. This proves to be rather useful as many integrable properties of a multivariate Gaussian can be leveraged in order to simplify the obtained expression. Such that for this work the variables used in Eq. (4.45), are also referred to as the closure coefficients of the distribution. As $\mathcal{F}$ takes the form of a multivariate Gaussian it can be shown that both $\hat{u}_i$, and $\hat{s}$ are the most-likely particle velocity and surface, or the peeks of the distribution. It is important to note that the peeks of the distribution do not represent the average velocity, μ_i and average surface, σ. Furthermore, while the tensor p_{ij}, vector q_{is}, and scalar r_{ss}, have an analogous representation to the variance-

covariance moments of the distribution, Θ_{ij}, Ψ_{is}, Ψ_{ss}, it is important not to interchange these variables. While the variance of particle velocity is given by the moment Θ_{ij}, and its value be can directly related to the closure coefficient corresponding to the particles variance of velocity, p_{ij} an important distinction needs to be made. The closure coefficient, p_{ij}, does not represent any moment or statistical property of the flow but rather dictates the shape of the distribution function, $\mathcal{F}$, of which can be integrated with appropriate weights in order to obtain its moments. By taking moments of the distribution function the closure coefficient can be related to the known macroscopic properties of the distribution that were derived in the previous section. By taking the moment, $w = 1$, of the distribution, $\mathcal{F}$, the number density can be expressed in terms of the closure coefficients,

$$\langle \mathcal{F} \rangle = n = 2\pi^2 \det(\boldsymbol{M})^{\frac{1}{2}} e^k \left(1 + \operatorname{erf}\left(\frac{\hat{s}}{\sqrt{2r_{ss}}}\right)\right) . \tag{4.47}$$

The average velocity, μ_i, and average surface, σ are given by

$$\langle v_i \mathcal{F} \rangle = n\mu_i = n\left(\hat{u}_i + \frac{q_{is}}{\sqrt{r_{ss}}}\mathcal{H}\right) , \tag{4.48}$$

$$\langle s \mathcal{F} \rangle = n\sigma = n\left(\hat{s} + \sqrt{r_{ss}}\mathcal{H}\right) . \tag{4.49}$$

In Eqs. (4.48)–(4.49), $\mathcal{H}$ is a common function found in the field of statics known as the hazard rate. The hazard rate, sometimes also called the inverse of the Mills ratio, is expressed as the ratio of the probability density function over its respective cumulative distribution function. For the PGM the $\mathcal{H}$ function can be expressed in terms of a ratio of two closure coefficients,

$$\mathcal{H}(\xi) = \frac{\sqrt{\frac{2}{\pi}} \exp\left[-\frac{1}{2}\xi^2\right]}{1 + \operatorname{erf}\left(\frac{1}{\sqrt{2}}\xi\right)} , \tag{4.50}$$

where ξ is the ratio of closure coefficients related to the particles surface, $\hat{s}$ and r_{ss},

$$\xi = \frac{\hat{s}}{\sqrt{r_{ss}}} . \tag{4.51}$$

In order to simplify the expressions of the obtained PDEs from the kinetic equation, it becomes useful to derive surface-weighted moments of the distribution function. These surface-weighted moments are taken by multiplying the original vector of weights by the surface, s such that the new vector of weights $\dot{\boldsymbol{\mathcal{W}}}$, is defined as the following,

$$\dot{\boldsymbol{\mathcal{W}}} = s\boldsymbol{\mathcal{W}} . \tag{4.52}$$

For these moments, the same symbols from the classical moments are maintained and decorated with dots in order to distinguish the surface-weighted moment variables. Such that, the surface-

Table 4.1: Table of Traditional Moments

Name	Weight	Moment	Closure Coefficient
Number Density	1	n	$2\pi^2 \det(\boldsymbol{M})^{\frac{1}{2}} e^k \left(1 + \operatorname{erf}\left(\frac{\hat{s}}{\sqrt{2r_{ss}}}\right)\right)$
Average Velocity	$\frac{v_i}{n}$	μ_i	$\hat{u}_i + \frac{q_{is}}{\sqrt{r_{ss}}}\mathcal{H}$
Average Surface	$\frac{s}{n}$	σ	$\hat{s} + \sqrt{r_{ss}}\mathcal{H}$
Velocity Variance	$\frac{1}{n}(v_i - \mu_i)(v_j - \mu_j)$	Θ_{ij}	$p_{ij} - q_{is}q_{js}\frac{\mathcal{H}}{r_{ss}^{3/2}}\sigma$
Covariance	$\frac{1}{n}(v_i - \mu_i)(s - \sigma)$	Ψ_{is}	$q_{is} - q_{is}\frac{\mathcal{H}}{\sqrt{r_{ss}}}\sigma$
Surface Variance	$\frac{1}{n}(s - \sigma)^2$	Ψ_{ss}	$r_{ss} - \sqrt{r_{ss}}\mathcal{H}\sigma$

Table 4.2: Table of Surface-Weighted (S-W) Moments

Name	Weight	Moment	Closure Coefficient
Surface Density	s	$\dot{n}$	$n\sigma$
S-W Average Velocity	$\frac{s v_i}{\dot{n}}$	$\dot{\mu}_i$	$\hat{u} + \frac{q_{is}}{\sigma}$
S-W Average Surface	$\frac{s^2}{\dot{n}}$	$\dot{\sigma}$	$\hat{s} + \frac{r_{ss}}{\sigma}$
S-W Velocity Variance	$\frac{s}{\dot{n}}(v_i - \dot{\mu}_i)(v_j - \dot{\mu}_j)$	$\dot{\Theta}_{ij}$	$p_{ij} + \frac{q_{is}q_{js}}{\sigma^2}\left(\frac{\mathcal{H}}{\sqrt{r_{ss}}}\sigma - 1\right)$
S-W Covariance	$\frac{s}{\dot{n}}(v_i - \dot{\mu}_i)(s - \dot{\sigma})$	$\dot{\Psi}_{is}$	$q_{is} + \frac{q_{is}r_{ss}}{\sigma^2}\left(\frac{\mathcal{H}}{\sqrt{r_{ss}}}\sigma - 1\right)$
S-W Surface Variance	$\frac{s}{\dot{n}}(s - \dot{\sigma})^2$	$\dot{\Psi}_{ss}$	$r_{ss} + \frac{r_{ss}^2}{\sigma^2}\left(\frac{\mathcal{H}}{\sqrt{r_{ss}}}\sigma - 1\right)$

weighted number density of the distribution function can be expressed as

$$\dot{n} = n\sigma = \langle s\mathcal{F} \rangle \ . \tag{4.53}$$

Much like the moment variables, the surface-weighted average velocity, $\dot{\mu}_i$ and surface-weighted average surface, $\dot{\sigma}$ can also be expressed in terms of the closure coefficients

$$\langle s\, v_i\, \mathcal{F} \rangle = \dot{n}\dot{\mu}_i = \dot{n}\left(\hat{u}_i + \frac{q_{is}}{\sigma}\right) , \tag{4.54}$$

$$\left\langle s^2\, \mathcal{F} \right\rangle = \dot{n}\dot{\sigma} = \dot{n}\left(\hat{s} + \frac{r_{ss}}{\sigma}\right) . \tag{4.55}$$

The higher-order moments and surface-weighted moments of the distribution function and their relationship to the closure coefficients can also be obtained by integrating over the distribution function, Eq. (4.45), while applying the correct weights. The obtained moments, with respect to the closure coefficients of $\mathcal{F}$ are outlined in Tables 4.1–4.3. Tables 4.1–4.3 present a guide to relate the name of the moment used in this paper to its respective weight and variable, along with their relationship to the closure-coefficient of $\mathcal{F}$. These tables prove to be quite useful in representing the PGM in closed form as the moment variables can be used in order to simplify the expressions

Table 4.3: Table of Skewness Moments

Name	Weight	Moment	Closure Coefficients
ijk Skewness	$\frac{1}{n}c_i c_j c_k$	Q_{ijk}	$q_{is}q_{js}q_{ks}\frac{\mathcal{H}}{r_{ss}^{5/2}}\left(\left(2\mathcal{H}^2-1\right)r_{ss}+3\hat{s}\sqrt{r_{ss}}\mathcal{H}+\hat{s}^2\right)$
ijk S-W Skewness	$\frac{s}{n}\dot{c}_i\dot{c}_j\dot{c}_k$	$\dot{Q}_{ijk}$	$\frac{q_{is}q_{js}q_{ks}}{\sigma}\left(\frac{2}{\sigma^2}-\frac{3\mathcal{H}}{\sqrt{r_{ss}}\sigma}-\frac{\hat{s}}{r_{ss}^{3/2}}\mathcal{H}\right)$
ijs Skewness	$\frac{1}{n}c_i c_j c_s$	Q_{ijs}	$q_{is}q_{js}r_{ss}\frac{\mathcal{H}}{r_{ss}^{5/2}}\left(\left(2\mathcal{H}^2-1\right)r_{ss}+3\hat{s}\sqrt{r_{ss}}\mathcal{H}+\hat{s}^2\right)$
ijs S-W Skewness	$\frac{s}{n}\dot{c}_i\dot{c}_j\dot{c}_s$	$\dot{Q}_{ijs}$	$\frac{q_{is}q_{js}r_{ss}}{\sigma}\left(\frac{2}{\sigma^2}-\frac{3\mathcal{H}}{\sqrt{r_{ss}}\sigma}-\frac{\hat{s}}{r_{ss}^{3/2}}\mathcal{H}\right)$
iss Skewness	$\frac{1}{n}c_i c_s^2$	Q_{iss}	$q_{is}r_{ss}^2\frac{\mathcal{H}}{r_{ss}^{5/2}}\left(\left(2\mathcal{H}^2-1\right)r_{ss}+3\hat{s}\sqrt{r_{ss}}\mathcal{H}+\hat{s}^2\right)$
iss S-W Skewness	$\frac{s}{n}\dot{c}_i\dot{c}_s^2$	$\dot{Q}_{iss}$	$\frac{q_{is}r_{ss}^2}{\sigma}\left(\frac{2}{\sigma^2}-\frac{3\mathcal{H}}{\sqrt{r_{ss}}\sigma}-\frac{\hat{s}}{r_{ss}^{3/2}}\mathcal{H}\right)$

obtained in the set of PDEs yet they can still be related to the shape of the distribution function, $\mathcal{F}$ by relating the moments to the closure-coefficient of the system. The previously shown PGM in balance law form, Eqs. (4.38)–(4.43), can also be expressed for the set of surface-weighted moments, $\dot{\boldsymbol{\mathcal{W}}}$. Using the same assumed form of the distribution, Eq. (4.45), the obtained PGM in balance law form takes on the identical form to the equation for the regular vector of weights, $\boldsymbol{\mathcal{W}}$ with the caveat that all the moments in Eqs. (4.38)–(4.43) are to be replaced with their respective surface-weighted moments. In other words, the number density, n is to be replaced with the surface-density, $\dot{n}$ the average velocity, μ_i with the surface-weighted average velocity, $\dot{\mu}_i$, *etc.* .

4.2.5 Hyperbolicity of the PGM

As stated in Section 3.4, it is important that the set of PDEs that are generated from PGM remains hyperbolic. To begin, it can be evident to see that selecting a set of surface-base generating weights, $\boldsymbol{\mathcal{W}} = \left[1, v_i, v_i v_j, s, v_i s, s^2\right]$, admits a set of hyperbolic PDEs. As selection of the particle surface as an internal variable does not change the fact that the density potential remains a strictly convex positive-definite Hessian and the flux potential remains a Hessian matrix. The proof shown in the previous section remains identical for the current set of weights and as such the system of PDEs using the following set of the weights, $\boldsymbol{\mathcal{W}} = \left[1, v_i, v_i v_j, s, v_i s, s^2\right]$, remains hyperbolic. In order to simplify the PDEs obtained in closed form a set of surface-weighted weights was used to generate the PDEs. Therefore, one must show that the set of surface-weighted PDEs, that are generated with the set of surface-weighted weights, $\dot{\boldsymbol{\mathcal{W}}} = s\left[1, v_i, v_i v_j, s, v_i s, s^2\right]$, must also lead to a set of hyperbolic PDEs. To begin the balance law for the set of PDEs is written as

$$\frac{\partial}{\partial t}\left\langle \dot{\boldsymbol{\mathcal{W}}}\mathcal{F}\right\rangle + \frac{\partial}{\partial x_\alpha}\left\langle v_\alpha \dot{\boldsymbol{\mathcal{W}}}\mathcal{F}\right\rangle = \left\langle a_\alpha \mathcal{F}\frac{\partial}{\partial v_\alpha}\dot{\boldsymbol{\mathcal{W}}}\right\rangle - \sum_{\check{i}=0}\left\langle \frac{\partial}{\partial \zeta_{\check{i}}}\left(\dot{\boldsymbol{\mathcal{W}}}\Upsilon_{\check{i}}\mathcal{F}\right)\right\rangle + \sum_{\check{i}=0}\left\langle \Upsilon_{\check{i}}\mathcal{F}\frac{\partial}{\partial \zeta_{\check{i}}}\dot{\boldsymbol{\mathcal{W}}}\right\rangle . \quad (4.56)$$

As the vector of surface-weighted weights can be expressed as, $\dot{\boldsymbol{\mathcal{W}}} = s\boldsymbol{\mathcal{W}}$, Eq. (4.56) can be written as

$$\frac{\partial}{\partial t}\left\langle s\boldsymbol{\mathcal{W}}\mathcal{F}\right\rangle + \frac{\partial}{\partial x_\alpha}\left\langle v_\alpha s\boldsymbol{\mathcal{W}}\mathcal{F}\right\rangle = \left\langle a_\alpha\mathcal{F}\frac{\partial}{\partial v_\alpha}s\boldsymbol{\mathcal{W}}\right\rangle - \sum_{\check{i}=0}\left\langle\frac{\partial}{\partial\zeta_{\check{i}}}\left(s\boldsymbol{\mathcal{W}}\Upsilon_{\check{i}}\mathcal{F}\right)\right\rangle + \sum_{\check{i}=0}\left\langle\Upsilon_{\check{i}}\mathcal{F}\frac{\partial}{\partial\zeta_{\check{i}}}s\boldsymbol{\mathcal{W}}\right\rangle . \tag{4.57}$$

One can derive the new surface-weighted balance law in order to obtain the density and flux potential,

$$h(\boldsymbol{\alpha})_{,\boldsymbol{\alpha},\boldsymbol{\alpha}}\frac{\partial\boldsymbol{\alpha}}{\partial t} + f_i(\boldsymbol{\alpha})_{,\boldsymbol{\alpha},\boldsymbol{\alpha}}\frac{\partial\boldsymbol{\alpha}}{\partial x_\alpha} = \boldsymbol{S} . \tag{4.58}$$

where the definition of the density and flux potential now have a surface-weighted value,

$$h(\boldsymbol{\alpha})_{,\boldsymbol{\alpha},\boldsymbol{\alpha}} = \left\langle s\boldsymbol{\mathcal{W}}\boldsymbol{\mathcal{W}}^T\mathcal{F}\right\rangle , \tag{4.59}$$

$$f_i(\boldsymbol{\alpha})_{,\boldsymbol{\alpha},\boldsymbol{\alpha}} = \left\langle sv_i\boldsymbol{\mathcal{W}}\boldsymbol{\mathcal{W}}^T\mathcal{F}\right\rangle . \tag{4.60}$$

One can notice that no matter the values in $\boldsymbol{\mathcal{W}}$ the product of the vector of weights with it self always admits a positive semi-definite matrix. Therefore, since the distribution function, $\mathcal{F}$ still takes the same form as the previous exponential, and that the defined surface area of a particle must be positive, the density potential, $h(\boldsymbol{\alpha})_{,\alpha,\alpha}$, must be a convex and positive-definite. Additionally, the flux potential, $f_i(\boldsymbol{\alpha})_{,\boldsymbol{\alpha},\boldsymbol{\alpha}}$, due to the inner product of the vector of weights, is a Hermitian matrix. Thus due to the positive definiteness of the density potential and the symmetry of the flux potential the system of PDEs is guaranteed to be hyperbolic.

4.3 Source Term

The source term present in the balance equation for the PGM is defined as

$$\boldsymbol{S} = \left\langle a_\alpha\mathcal{F}\frac{\partial}{\partial v_\alpha}\boldsymbol{\mathcal{W}}\right\rangle - \left\langle\frac{\partial}{\partial\zeta_{\check{i}}}\boldsymbol{\mathcal{W}}\Upsilon_{\check{i}}\mathcal{F}\right\rangle + \left\langle\Upsilon_{\check{i}}\mathcal{F}\frac{\partial}{\partial\zeta_{\check{i}}}\boldsymbol{\mathcal{W}}\right\rangle . \tag{4.61}$$

For the scope of this work, a simple model is considered with particles taking on the form of a uniform sphere and the fluid is assumed to follow the Stokes-flow approximation, such that the acceleration felt by the particles in the system will follow Eq. (2.3). The source term also captures the rate of change of the studied internal variable, $\zeta_{\check{i}}$. As the selected internal variable is the particles surface area the rate of change of the surface, $\Upsilon_{\check{i}}$, can be described from the steady-state linear evaporation rate for spherical particles, Eq. (2.6).

4.3.1 Source Term for the Log-Normal PGM

For the originally proposed PGM model, the logarithm of particle diameter is chosen as the sole distinguishing variable. Leading to preivously shown set of weights, $\boldsymbol{\mathcal{W}}_D$. This choice leads to a very nice model described by simple, closed-form balance laws with $Q_{ijk} = 0$, clean known wave speeds, and a simple entropy [5]. The resulting right-hand side for the moment equations, $\boldsymbol{S}$, is

given by

$$\boldsymbol{S_d} = \begin{bmatrix} S_d^{(1)} \\ S_d^{(2)} \\ S_d^{(3)} \\ S_d^{(4)} \\ S_d^{(5)} \\ S_d^{(6)} \end{bmatrix}, \tag{4.62}$$

$$S_d^{(1)} = 0\,, \tag{4.63}$$

$$S_d^{(2)} = \frac{n}{\tau_{\mathcal{G}}}\left(V_i - (\mu_i - 2\Psi_{id})\right) + n\phi_i\,, \tag{4.64}$$

$$\begin{aligned} S_d^{(3)} = {} & \frac{n}{\tau_{\mathcal{G}}}\left(V_i(\mu_j - 2\Psi_{jd}) + V_j(\mu_i - 2\Psi_{id})\right) \\ & -2\frac{n}{\tau_{\mathcal{G}}}\left(\mu_i\mu_j - 2\mu_i\Psi_{jd} - 2\mu_j\Psi_{id} + 4\Psi_{id}\Psi_{jd} + \Theta_{ij}\right) + n\left(\mu_j\phi_i + \mu_i\phi_j\right)\,, \end{aligned} \tag{4.65}$$

$$S_d^{(4)} = 0\,, \tag{4.66}$$

$$S_d^{(5)} = \frac{n}{\tau_{\mathcal{G}}}\left(V_i\left(\mu_d - 2\Psi_{dd}\right) - \left(\mu_d\mu_i - 2\mu_d\Psi_{id} - 2\mu_i\Psi_{dd} + 4\Psi_{dd}\Psi_{id} + \Psi_{id}\right)\right) + n\mu_d\phi_i\,, \tag{4.67}$$

$$S_d^{(6)} = 0\,. \tag{4.68}$$

In these expressions,

$$\tau_{\mathcal{G}} = \frac{\rho_p}{18\mu f}e^{(2\mu_d - 2\Psi_{dd})}\,, \tag{4.69}$$

and the "d" subscript is used to denote moments related to the logarithm of the particle diameter.

4.3.2 Source Term for the Surface-Based PGM

For the surface-weighted moments, $\dot{\boldsymbol{W}}$, with a consideration for particle evaporation the right-hand side of the moment equation, $\dot{\boldsymbol{S}}$, is given in closed-form as

$$\dot{\boldsymbol{S}} = \begin{bmatrix} \dot{S}^{(1)} \\ \dot{S}_i^{(2)} \\ \dot{S}_{ij}^{(3)} \\ \dot{S}_s^{(4)} \\ \dot{S}_{si}^{(5)} \\ \dot{S}_{ss}^{(6)} \end{bmatrix}, \tag{4.70}$$

$$\dot{S}^{(1)} = -n\alpha\pi\,, \tag{4.71}$$

$$\dot{S}_i^{(2)} = \frac{n}{\gamma}\left(V_i - \mu_i\right) + \dot{n}\phi_i - n\alpha\pi\mu_i\,, \tag{4.72}$$

$$\dot{S}_{ij}^{(3)} = \frac{n}{\gamma}\left(V_i\mu_j + V_j\mu_i - 2\left(\Theta_{ij} + \mu_i\mu_j\right)\right) + \dot{n}\left(\phi_i\mu_j + \phi_j\mu_i\right) - n\alpha\pi\left(\Theta_{ij} + \mu_i\mu_j\right)\,, \tag{4.73}$$

$$\dot{S}_s^{(4)} = -2\dot{n}\alpha\pi\,, \tag{4.74}$$

$$\dot{S}_{si}^{(5)} = \frac{\dot{n}}{\gamma}\left(V_i - \dot{\mu}_i\right) + \dot{n}\dot{\sigma}\phi_i - 2\dot{n}\alpha\pi\dot{\mu}_i\,, \tag{4.75}$$

$$\dot{S}_{ss}^{(6)} = -3\dot{n}\alpha\pi\dot{\sigma}\,. \tag{4.76}$$

In Eq. (4.70), γ is defined as the relaxation parameter due to drag and contains all the constant properties of the particles in the flow and is given by

$$\gamma = \frac{\rho_p}{18\pi\mu_f}\,. \tag{4.77}$$

It is important to note that, in order to simplify the PDEs, the source term is given as a mix of both moment and surface-weighted moment variables. Both can be related to the closure coefficients presented in Tables 4.1–4.3. Additionally the source term can also be presented in its primitive form,

$$\frac{\partial\dot{n}}{\partial t} = \dot{S}^{(1)}\,, \tag{4.78}$$

$$\frac{\partial\dot{\mu}_i}{\partial t} = \frac{1}{\dot{n}}\left(\dot{S}_i^{(2)} - \dot{\mu}_i\dot{S}^{(1)}\right)\,, \tag{4.79}$$

$$\frac{\partial\dot{\Theta}_{ij}}{\partial t} = \frac{1}{\dot{n}}\left(\dot{S}_{ij}^{(3)} - \left(\dot{\Theta}_{ij} + \dot{\mu}_i\dot{\mu}_j\right)\dot{S}^{(1)} - \dot{\mu}_i\dot{S}_j^{(2)} - \dot{\mu}_j\dot{S}_i^{(2)} + 2\dot{\mu}_i\dot{\mu}_j\dot{S}^{(1)}\right)\,, \tag{4.80}$$

$$\frac{\partial\dot{\sigma}}{\partial t} = \frac{1}{\dot{n}}\left(\dot{S}_s^{(4)} - \dot{\sigma}\dot{S}^{(1)}\right)\,, \tag{4.81}$$

$$\frac{\partial\dot{\Psi}_{is}}{\partial t} = \frac{1}{\dot{n}}\left(\dot{S}_{is}^{(5)} - \left(\dot{\Psi}_{is} + \dot{\mu}_i\dot{\sigma}\right)\dot{S}^{(1)} - \dot{\sigma}\dot{S}_i^{(2)} - \dot{\mu}_i\dot{S}_s^{(4)} + 2\dot{\mu}_i\dot{\sigma}\dot{S}^{(1)}\right)\,, \tag{4.82}$$

$$\frac{\partial\dot{\Psi}_{ss}}{\partial t} = \frac{1}{\dot{n}}\left(\dot{S}_{ss}^{(6)} - \left(\dot{\Psi}_{ss} + \dot{\sigma}^2\right)\dot{S}^{(1)} - 2\dot{\sigma}\dot{S}_s^{(4)} + 2\dot{\sigma}^2\dot{S}^{(1)}\right)\,, \tag{4.83}$$

$$\tag{4.84}$$

4.4 Space-Homogeneous Steady-State Solution for Particles Settling in Stokes Flow

One of the main focus of the thesis was to capture particle settling exactly and as such a simplified space-homogeneous case is considered. In a simplified space-homogeneous case, without evaporation, the governing PDEs of the surface based PGM can be expressed as a set of ordinary

differential equations (ODEs) in their primitive form Eq. (4.70) as

$$\dot{n}\frac{\mathrm{d}\dot{\mu}_i}{\mathrm{d}t} = \dot{S}_i^{(2)}\,, \tag{4.85}$$

$$\dot{n}\frac{\mathrm{d}\dot{\Theta}_{ij}}{\mathrm{d}t} = \dot{S}_{ij}^{(3)} - \dot{\mu}_i\dot{S}_j^{(2)} - \dot{\mu}_j\dot{S}_i^{(2)}\,, \tag{4.86}$$

$$\dot{n}\frac{\mathrm{d}\dot{\Psi}_{is}}{\mathrm{d}t} = \dot{S}_{is}^{(5)} - \dot{\sigma}\dot{S}_i^{(2)}\,. \tag{4.87}$$

Without evaporation the source terms $S^{(1)}$, $S_s^{(4)}$, $S_{ss}^{(6)}$, are zero, making the moment variables, $\dot{n}$, $\dot{\sigma}$ and $\dot{\Psi}_{ss}$ time invariant,

$$\frac{\mathrm{d}\dot{n}}{\mathrm{d}t} = 0\,, \tag{4.88}$$

$$\frac{\mathrm{d}\dot{\sigma}}{\mathrm{d}t} = 0\,, \tag{4.89}$$

$$\frac{\mathrm{d}\dot{\Psi}_{ss}}{\mathrm{d}t} = 0\,. \tag{4.90}$$

These ODEs, Eqs. (4.85)–(4.87) can be expressed in terms of the moments of the distribution function,

$$\frac{\mathrm{d}\dot{\mu}_i}{\mathrm{d}t} = \frac{1}{\gamma\sigma}\left(V_i - \mu_i\right) + \phi_i\,, \tag{4.91}$$

$$\frac{\mathrm{d}\dot{\Theta}_{ij}}{\mathrm{d}t} = \frac{1}{\gamma\sigma}\left(V_i\mu_j + V_j\mu_i - 2\left(\Theta_{ij} + \mu_i\mu_j\right) - \dot{\mu}_i\left(V_j - \mu_j\right) - \dot{\mu}_j\left(V_i - \mu_i\right)\right)\,, \tag{4.92}$$

$$\frac{\mathrm{d}\dot{\Psi}_{is}}{\mathrm{d}t} = \frac{1}{\gamma}\left(\left(V_i - \dot{\mu}_i\right) - \frac{\dot{\sigma}}{\sigma}\left(V_i - \mu_i\right)\right)\,. \tag{4.93}$$

It is important to note that Eqs. (4.91)–(4.93) are presented as a mix of weighted and non-weighted moment variables of the PGM. As previously mentioned, these moment variables can be related to the closure coefficients of the distribution in order to describe the evolution of the distribution, $\mathcal{F}$, over time.

For spherical particles settling in a Stokes flow it is known that the terminal velocity of a particle can be described with

$$v_i = \frac{s}{18\pi\mu_f}(\rho_p - \rho_f)g_i = \gamma\phi_i s\,, \tag{4.94}$$

where v_i is the terminal velocity of a particle with given surface area, s, particle density, ρ_p, in a given fluid with density, ρ_f, and dynamic viscosity, μ_f, and subject to gravity g_i. For a space-homogeneous situation of particles settling in a quiescent background, the moments of the

original PGM reach a steady, terminal state described by

$$\mu_i = \phi_i \tau_{\mathcal{G}} (1 + 4\Psi_{dd}) \,, \tag{4.95}$$

$$\Theta_{ij} = 4\phi_i \phi_j \tau_{\mathcal{G}}^2 \Psi_{dd} \,, \tag{4.96}$$

$$\Psi_{id} = 2\phi_i \tau_{\mathcal{G}} \Psi_{dd} \,. \tag{4.97}$$

However, without the moment approximation imposed by the assumed distribution function, a collection of particles with a log-normal distribution of diameters would actually reach a terminal steady state of

$$\mu_i = \phi_i \, \tau_{\mathcal{G}} \, e^{4\Psi_{dd}} \,, \tag{4.98}$$

$$\Theta_{ij} = \phi_i \phi_j \, {\tau_{\mathcal{G}}}^2 \, e^{8\Psi_{dd}} \left(e^{4\Psi_{dd}} - 1 \right) \,, \tag{4.99}$$

$$\Psi_{id} = 2\phi_i \, \tau_{\mathcal{G}} \, \Psi_{dd} e^{4\Psi_{dd}} \,. \tag{4.100}$$

Through a Taylor-series expansion, one case see that, for small values of Ψ_{dd}, the correct solution agrees with the moment approximation. However, as this variance increases, deviations grow. It is this inability of the original PGM to correctly predict the particle settling rate that initially motivated the development of the new closure based on the particle surface area.

As Eq. (4.94) contains the particles surface, s, and Stokes flow reaches a steady-state distribution that is inversely proportional the surface area of a particle one can infer that taking the surface-based moments the distribution function should recover the exact solution. In order to confirm that the steady-state solution is indeed recovered the weighted-moment variables at steady state can be evaluated then compared with the known steady-state velocity. The moments

$$\dot{n}\dot{\mu}_i = \langle s v_i \mathcal{F} \rangle \,, \tag{4.101}$$

$$\dot{n}\dot{\Theta}_{ij} = \langle s (v_i - \dot{\mu}_i)(v_j - \dot{\mu}_j) \mathcal{F} \rangle \,, \tag{4.102}$$

$$\dot{n}\dot{\Psi}_{is} = \langle s (v_i - \dot{\mu}_i)(s - \dot{\sigma}) \mathcal{F} \rangle \,, \tag{4.103}$$

with v_i set to the known settling terminal velocity, Eq. (4.94) can then be compared to the moments obtained at local equilibrium from the set of ODEs in Eqs. (4.91)–(4.93). It can be shown that the set of ODEs from the model recover the exact steady-state solution obtained from the kinetic equations,

$$\dot{\mu}_i = \phi_i \gamma \dot{\sigma} \,, \tag{4.104}$$

$$\dot{\Theta}_{ij} = \phi_i \phi_j \gamma^2 \dot{\Psi}_{ss} \,, \tag{4.105}$$

$$\dot{\Psi}_{is} = \phi_i \gamma \dot{\Psi}_{ss} \,. \tag{4.106}$$

One can observe that the moment corresponding to the terminal velocity, Eq. (4.104) states that particles settle at an average terminal velocity for a given initial average surface, $\dot{\sigma}$. Furthermore, the spread of that settling terminal velocity, Eq. (4.105), is governed by the initial spread of par-

ticle surface, $\dot{\Psi}_{ss}$. The same can also be said about Eq. (4.106), this equation refers to the settling covariance of the particles velocity and surface and is directly related to the parameters of the fluid, ϕ_i and γ and the initial spread of particle size, $\dot{\Psi}_{ss}$. These are in perfect agreement with the exact solution of the kinetic equation with a distribution function for particles that have normally distributed surface areas. This agreement between the surface-based PGM and the kinetic equation for settling particles is further demonstrated in Section 7.1.

Chapter 5

Efficient Kinetic Solver

In order to validate the results obtained from the PGM, a numerical Kinetic solver was also developed. This numerical solver, while extremely slow when used to obtain the exact solution to a high-dimensional problem, can be used to obtain solutions to moments of a wide range of kinetic equations. In simple cases, such as a space-homogeneous case this solver can be used to validate the accuracy of the PGM. Computation of the solutions becomes orders of magnitude more expensive to obtain as the degrees of freedom of the system increases. In the case of the full surface-weighted PGM, since this problem is in three spacial dimensions, three velocity dimensions, and a surface dimension obtaining the exact numerical solution becomes extremely computationally expensive. As such this solver cannot be feasibly used to compute solutions to a three-dimensional case, but rather used in order to validate numerical results of simpler problems.

5.1 Numerical Solution of the Kinetic Equation

To begin, the generic kinetic equation of interest is the previously shown kinetic equation with no collisions and a set of distinct variables

$$\frac{\partial \mathcal{F}}{\partial t} + v_\alpha \frac{\partial \mathcal{F}}{\partial x_\alpha} + \frac{\partial}{\partial v_\alpha}\left(a_\alpha \mathcal{F}\right) + \sum_{\check{i}=0} \frac{\partial}{\partial \zeta_{\check{i}}}\left(\Upsilon_{\check{i}} \mathcal{F}\right) = 0\,. \tag{5.1}$$

It is important to note that collisions are not considered for this kinetic equation, Eq. (5.1), as the inclusion of the collision operator changes the properties of the kinetic equations such that it is no longer reversible. The importance of having a reversible kinetic equation is explained in the following section. The set of kinetic equations, of which this solver aims to solve, Eq. (5.1) can be expressed in a Lagrangian form as

$$\frac{D\mathcal{F}}{Dt} = -\mathcal{F}\left(\frac{\partial}{\partial v_\alpha}\left(a_\alpha\right) + \sum_{\check{i}=0} \frac{\partial}{\partial \zeta_{\check{i}}}\left(\Upsilon_{\check{i}}\right)\right). \tag{5.2}$$

Eq. (5.2), described a particles trajectory through phase space. These trajectories are the solutions to

$$\frac{\mathrm{d}}{\mathrm{d}t}\begin{bmatrix} x_i \\ v_i \\ \zeta_{\check{i}} \end{bmatrix} = \begin{bmatrix} v_i \\ a_i \\ \Upsilon_{\check{i}} \end{bmatrix} . \tag{5.3}$$

In Eq. (5.3), a_i, and $\Upsilon_{\check{i}}$, are prescribed functions of x_i, v_i, $\zeta_{\check{i}}$. In the implementation of the PGM these functions take the form of those described in Chapter 2, Eqs. (2.3)–(2.3). Given a set of states at time t,

$$\Phi_t = \left[x_i,\ v_i,\ \zeta_{\check{i}}, t\right] , \tag{5.4}$$

the phase-space density can be obtain via means of the distribution function $\mathcal{F}$,

$$n_t = \mathcal{F}\left(\Phi_t\right) . \tag{5.5}$$

More notably the evolution of the state of these particles and their density can be described by combining Eq. (5.2) with Eq. (5.3), such that one obtains

$$\frac{\mathrm{d}}{\mathrm{d}t}\begin{bmatrix} x_i \\ v_i \\ \zeta_{\check{i}} \\ \mathcal{F} \end{bmatrix} = \begin{bmatrix} v_i \\ a_i \\ \Upsilon_{\check{i}} \\ -\mathcal{F}\left(\frac{\partial}{\partial v_\alpha}\left(a_\alpha\right) + \sum_{\check{i}=0} \frac{\partial}{\partial \zeta_{\check{i}}}\left(\Upsilon_{\check{i}}\right)\right) \end{bmatrix} . \tag{5.6}$$

As the expressions for the prescribed functions of x_i, v_i, $\zeta_{\check{i}}$ have already been determined for the PGM, the derivatives in the final term, $\frac{\partial a_\alpha}{\partial v_\alpha}$ and $\frac{\partial \Upsilon_{\check{i}}}{\partial \zeta_{\check{i}}}$, can be easily computed using algorithmic differentiation. Thus, in order to obtain the solution at a given time, one can use any standard time-marching method for Eq. (5.6).

5.1.1 Kinetic Solver, Forward Mode

The solver in its forward mode simply functions by taking in a initial state of the distribution, Φ_0, and a set of governing equations describing how the states Φ evolves with time. At the final state, one has to compute the moments from the given states, Φ_t. To begin, the initial conditions are selected such that a state vector, Φ_0, can be used to represent the current state of the solver. The initial state of $\mathcal{F}$ must thus be described by

$$\mathcal{F}_0 = \mathcal{F}\left(x_{i_0},\ v_{i_0},\ \zeta_{\check{i}_0}, 0\right) = \mathcal{F}\left(\Phi_0\right) . \tag{5.7}$$

In addition to the initial state vector be recorded at the start of the time marching process the initial phase-space density must also be recorded. This is because as time progresses it is very likely that the density in space changes. This change is density can be interpreted as a "stretching" of the distribution $\mathcal{F}$. This change is density is already been described by Eq. (5.2). At the initial

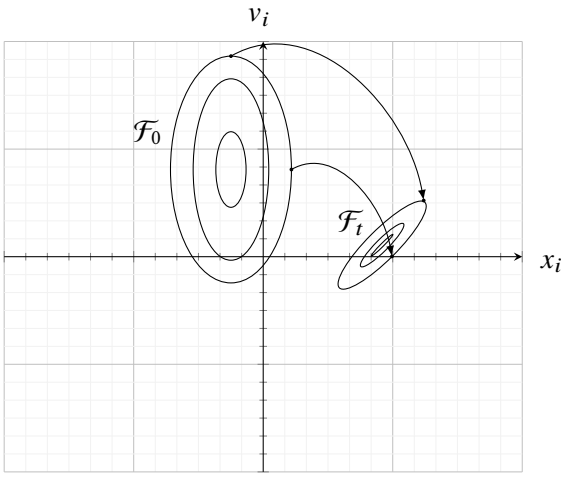

Figure 5.1: Evolution of the distribution function in phase space

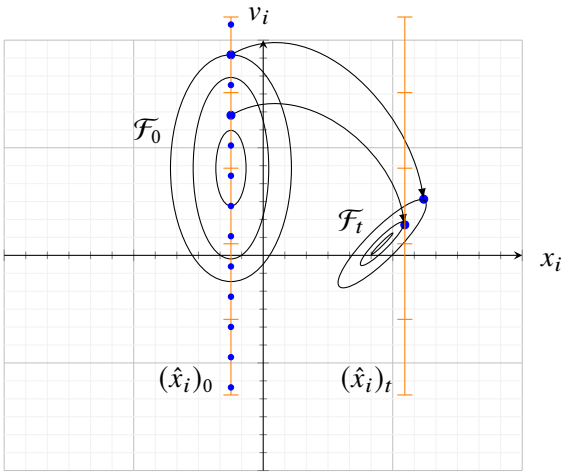

Figure 5.2: Moments of $\mathcal{F}_t$ on a Cartesian mesh

conditions, in order to in order to satisfy Eq. (5.2), such that

$$\mathcal{F}_0 = \mathcal{F}\left(\Phi_0\right) , \tag{5.8}$$

the initial value of $\mathcal{F}$ is the following

$$\mathcal{F}_0 = 1 . \tag{5.9}$$

The next step is to solve for the set of governing PDEs of the system, Eq. (5.6), using any standard time-marching method. Figure 5.1 illustrates how an initial distribution might relax to a certain state after a given time interval. One can notice how the phase-space density of $\mathcal{F}$ might change after a given time interval. This can be interpreted visually as a "stretching" of the distribution. In the presented figure the initial sampling points for $\mathcal{F}_0$ are placed are a Cartesian mesh, moments of $\mathcal{F}_0$ can be simply obtained from the initial conditions and the initial phase-space density that is known. The issue arises when attempting to obtain the moments of the distribution at a given future time. Figure 5.2 illustrates the initial distribution with and example of possible initial

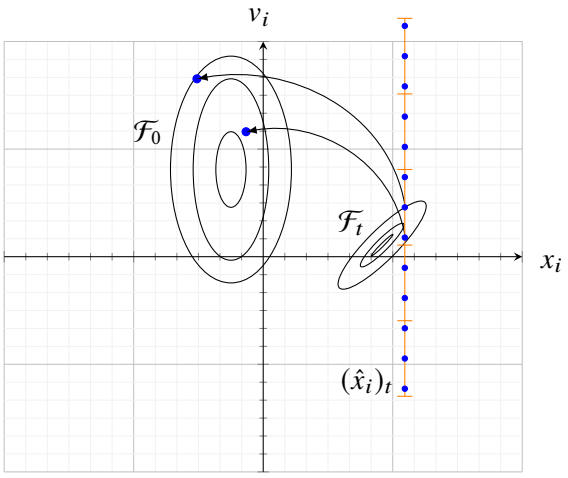

Figure 5.3: Quadrature points, backwards-mode

quadrature points used to evaluate the initial distribution function (shown in blue). One can see how these initial quadrature points that will be time-marched to a desired final state might relax on to the mesh, shown in orange. If one where to compute the moments of $\mathcal{F}_t$ at a given position $(\hat{x}_i)_t$ it is improbable that the initial quadrature points land exactly onto the desired sampled location of the moments, $(\hat{x}_i)_t$. In order to obtain those moments, sets of higher order interpolations has to be preformed on the final quadrature points. It is for this reason that the exact kinetic solver was implemented in a backwards mode.

5.1.2 Kinetic Solver, Backwards Mode

The kinetic solver, in order to obtain the exact solution to the moments of any given kinetic equations, functions in a reverse fashion. For this implementation of the solver it is assumed that the initial distribution, $\mathcal{F}_0$ is known and the final state of the distribution, $\mathcal{F}_t$ along with its moments is what the solver aims to determine. To being, final states are selected in the domain as the starting condition of the solver. This initial domain correspond to the quadrature points placed in blue on Figure 5.3. The previously shown PDEs, Eq. (5.6) can be solved in reverse in order to determine the initial states of all the selected starting conditions, provided that all the equations are reversible in nature. Such that using any time-marching technique, Φ_0, and $\mathcal{F}_0$, can be obtained from Φ_t. The elegance of the backwards mode solver comes from the following, by solving the set of PDEs in reverse order along the characteristics one obtains not only the initial conditions of a each quadrature point that would have lead them to the state Φ_t, but the final state of the distribution can be obtained, $\mathcal{F}_t$ at the initially placed quadrature points by solving for

$$\mathcal{F}_t = \frac{\mathcal{F}_0}{\mathcal{F}}, \tag{5.10}$$

where $\mathcal{F}$ is obtained by solving the Lagrangian as described in Eq. (5.6).

Furthermore, since the current state, Φ_t, was used to obtain the distribution, $\mathcal{F}_t$, any set of moments can be computed after obtaining the "stretching" factor of the distribution. This provides

a simple yet elegant solution to obtaining all the needed moments of the system as the selection of the initial states can be implemented quite trivially in a completely independent manner. This means that the implementation of this exact solver can be easily parallelized such that it would yield incredibly scalability on a distributed computing system.

The implementation of the exact moment solver does come with a catch due to its implementation. That is, the user must have an intuition as to the final state of the distribution. As sections of the backwards mode initial conditions, Φ_t requires knowledge of the shape of the final distribution in order to yield a possible final state given the initial distribution, $\mathcal{F}_0$ one must be careful in the selection of Φ_t. If an inadequate selection of the initial state, Φ_t is made it can results in missed information in computing the moments of the system or one could in theory select a state, Φ_t that is impossible to reach given the initial distribution, $\mathcal{F}_0$.

Chapter 6

Numerical Methods

This chapter presents the numerical methods implemented and used in this thesis to find solutions to the PGM. This section includes the complexity that one might encounter when implementing the conversion of the closure-coefficients to the to moment variables of the PGM or *vice versa* and presents the numerical techniques implemented in computation of these moments. Additionally, numerical techniques used in obtaining results for simple space-homogeneous cases, in addition to more complex three-dimensional cases are discussed in this chapter.

6.1 Computation of the Mills Ratio

One of the crucial components of the PGM is being able translate between the closure coefficient and the moment variables. This is done with the use of the relation given in Tables 4.1–4.3. From these tables, one can develop an understanding of the role $\mathcal{H}$ plays on the probability density function. In order to illustrate these numerical dependencies it can be useful to represent the $\mathcal{H}$ function in its more traditional form, often found in the field of statistics [1, 25]. The hazard ratio or the inverse of the Mills ratio is often represented as the ratio of the probability density function to its respective cumulative distribution,

$$\mathcal{H}(\xi) = \frac{\phi(\xi)}{\Phi(\xi)} \,. \tag{6.1}$$

For the presented work, ϕ is a normal Gaussian probability density function of ξ, such that

$$\phi(\xi) = \frac{1}{\sqrt{2\pi}} e^{-\frac{1}{2}\xi^2} \,, \tag{6.2}$$

and Φ is its respective cumulative distribution,

$$\Phi(\xi) = \frac{1}{2}\left(1 + \operatorname{erf}\left(\frac{\xi}{\sqrt{2}}\right)\right) \,. \tag{6.3}$$

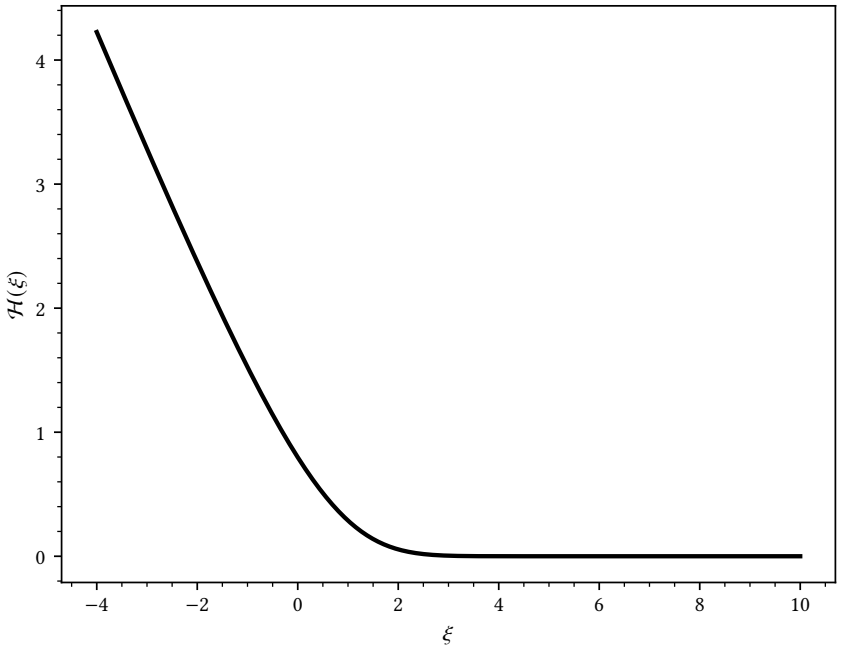

Figure 6.1: Computation of the Hazard function

In the case of the PGM, the random variable, ξ, is given by a ratio of the closure coefficients corresponding to the particles surface area,

$$\xi = \frac{\hat{s}}{\sqrt{r_{ss}}} \,. \tag{6.4}$$

From the tables of computed moments (Tables 4.1–4.3) the relationship between the closure coefficients and the moment variable corresponding to the particles average surface is given by,

$$\sigma = \hat{s} + \sqrt{r_{ss}}\mathcal{H}(\xi) \,. \tag{6.5}$$

With the hazard function plotted in Figure 6.1, one can develop an understanding of the relationship between the closure coefficients and the moment variables of the distribution function. For large positive values of ξ, such that the ratio of the peak of the distribution, $\hat{s}$, is much larger than the closure coefficient r_{ss}, the value of the hazard ratio approaches zero. From Eq. (6.5) this means that the closure coefficient, $\hat{s}$, becomes equal to the moment variable σ. In a more statistics based representation, one could say the peak of the particle distribution corresponds to the average particle surface. This only happens for large positive values of $\hat{s}$ and when the closure coefficient r_{ss} is very small resulting in a large value of ξ. The system would be such that the particle sizes are tightly coupled to a large positive value of $\hat{s}$. When the value of ξ approaches zero from the positive direction the gap between the closure coefficient $\hat{s}$ and the moment σ widen. This is due to the fact that a more significant amount of the tail of the normal Gaussian distribution is passing the location of truncation ($\xi = 0$). As the truncated Gaussian distribution cannot extend

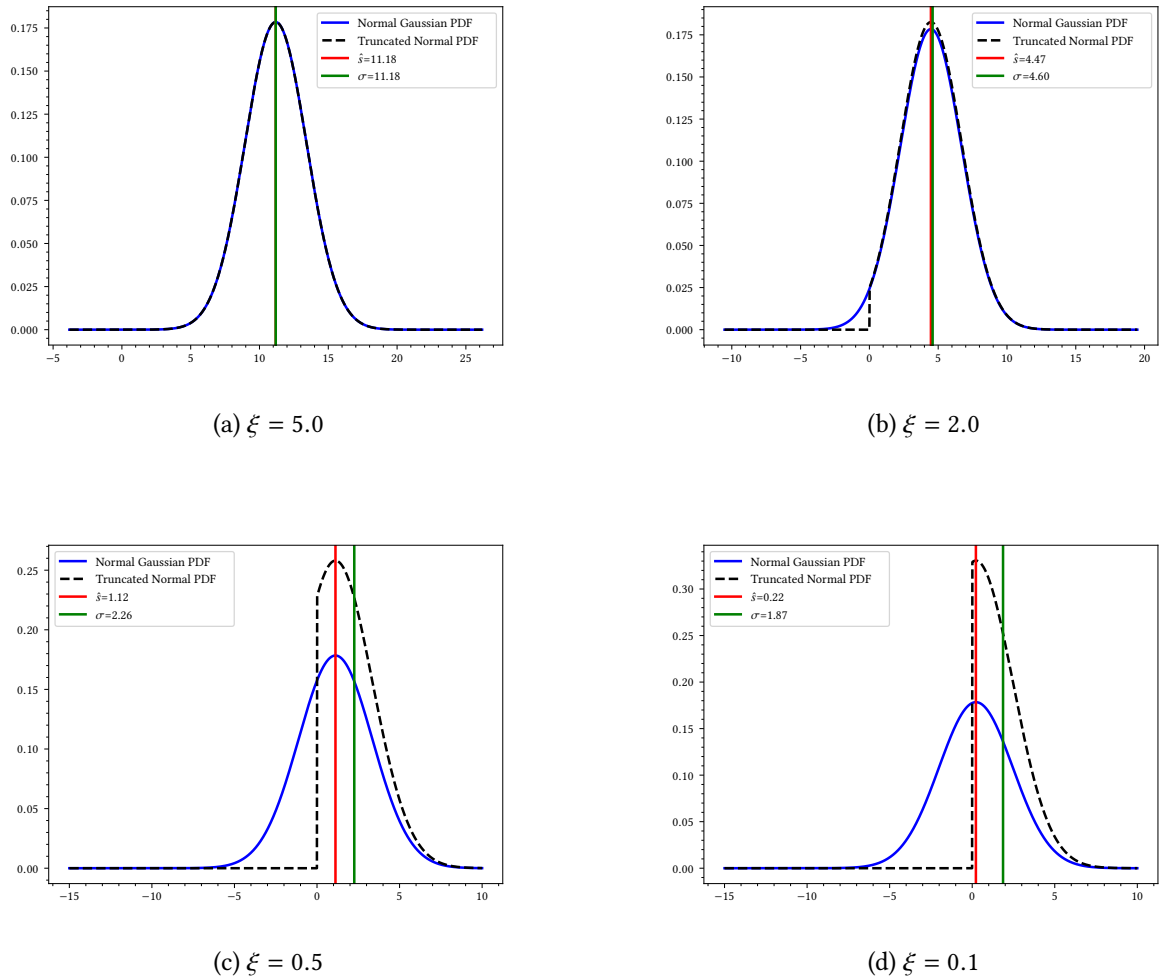

(a) $\xi = 5.0$

(b) $\xi = 2.0$

(c) $\xi = 0.5$

(d) $\xi = 0.1$

Figure 6.2: Truncated and Normal Gaussian PDF for various values of ξ

into the negative ξ space, σ starts to take on values that are further away fromt he closure coefficient, $\hat{s}$. Figure 6.2, illustrates this transition by plotting the truncated normal distribution with its respective normal Gaussian distributions for various values of ξ. In the presented figures the total number density and the variance of the Gaussian distributions are maintained constant and are set to 1 and 5 respectively. In Figure 6.2, one can notice that, once a significant portion of the normal distribution crosses zero, the gap between the closure coefficient, $\hat{s}$ and the moment σ becomes much more prevalent. It is important to note that it is possible that the closure coefficient of a given truncated moment admits a negative value, such as the case presented in in Figure 6.3. In Figure 6.3, the total number density and the variance of the Gaussian distributions are the same as presented Figure 6.2, and set to 1 and 5 respectively. In this case the closure coefficient, $\hat{s}$ is set to a negative value. One can notice that even for negative values of the closure coefficient, $\hat{s}$, the obtained moment of the truncated normal distribution, σ, is a positive value. In a physical sense this means that a solution of the PGM can admit a negative closure coefficient, $\hat{s}$, but it can be shown that it always admits a positive average surface, σ. Furthermore, the variance of the particle surface, Ψ_{ss} in addition to the closure coefficient r_{ss} it can be shown, due to the imposed

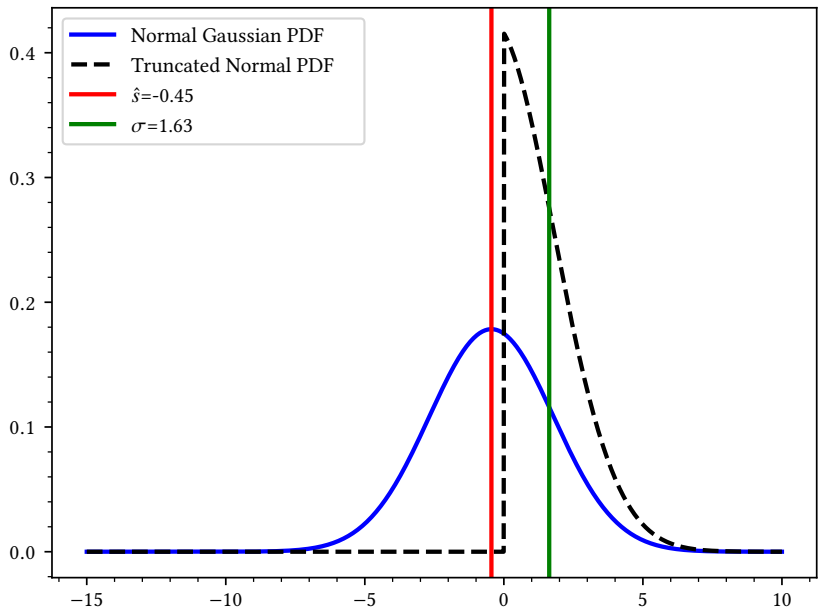

Figure 6.3: Truncated and Normal Gaussian PDF for $\xi = -0.2$

form of the distribution, $\mathcal{F}$, remains positive for any realizable value of the distribution. As the value of ξ tends towards greater negative numbers the moment, σ asymptotically approaches zero.

6.1.1 Numerical Difficulties with the $\mathcal{H}$ Function

The PGM, in the conserved form as presented in Eq. (3.19), is expressed using a mix of both closure coefficients and moment variables for both the surface and surface-weighted statistics. This means that, in order to solve for the conserved vector, both the flux and source term of the PGM must be evaluated in terms of the conserved variables, $\boldsymbol{U}$. As both the flux term and the source term are expressed in terms of the closure coefficients one must be able to convert reliably from the conserved moment variables to the closure coefficients and back. Conversion from the closure coefficients to the moment variables can be done by the use of the Tables 4.1–4.3. Going from the moment variables to the closure coefficients is, unfortunately, not as simple. Due to the non-linearity of the $\mathcal{H}$ function it is difficult to obtain an expression in closed form for the closure coefficients in terms of the moment variables. Thankfully, one can notice that there exists a coupling between the moments corresponding to the average and variance of the particles surface, σ and Ψ_{ss}. For instance, in the surface-weighted PGM the coupling is

$$\dot{\sigma} = \hat{s} + \frac{r_{ss}}{\sigma}, \tag{6.6}$$

$$\dot{\Psi}_{ss} = r_{ss} + \frac{r_{ss}^2}{\sigma^2}\left(\frac{\mathcal{H}}{\sqrt{r_{ss}}}\sigma - 1\right). \tag{6.7}$$

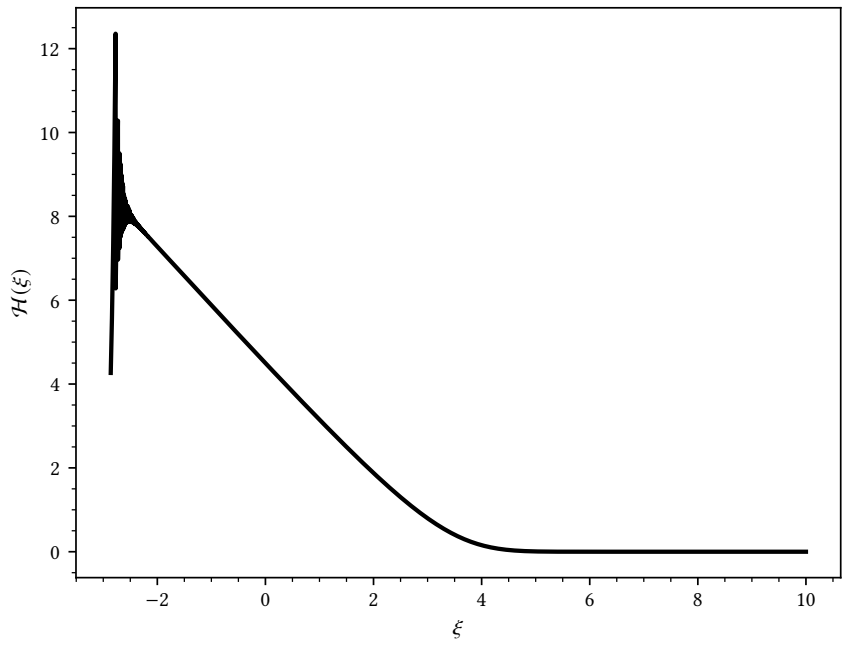

Figure 6.4: Error in Computation of $\mathcal{H}(\xi)$ using double precision

In Eqs. (6.6)–(6.7), both $\dot{\sigma}$ and $\dot{\Psi}_{ss}$ (weighted average and weighted variance of the particles surface area) are only a function of the closure coefficients $\hat{s}$ and r_{ss}. Such that, provided with the moment variables $\dot{\sigma}$ and $\dot{\Psi}_{ss}$, one could use a non-linear solver in order to obtain the closure coefficients $\hat{s}$ and r_{ss}. Once the closure coefficients related to the surface have been obtained, expressions for the remaining closure coefficients of the PGM can be obtained in closed form from the Tables 4.1–4.3. In practice this conversion from moment variables to the closure coefficients is very difficult to preform, as this problem can be very ill-conditioned numerically.

To begin, using double precision to evaluate the hazard function for values $\xi \lessapprox -6.0$ results in unacceptable numerical error. This makes even the forward evaluation, going from the closure coefficients to the moments of the PGM inaccurate for any situation where ξ is less than -6.0. Figure 6.4, illustrates that computing the hazard function for larger negative values becomes very difficult. This is because, while computing the probability density function does not generate any error for large negative values of ξ, computing the cumulative density function, and more precisely computing the error function for negative values of ξ becomes very difficult to preform with finite precision. In its limit the error function asymptotically reaches the value of -1,

$$\lim_{\xi \to -\infty} \operatorname{erf}(\xi) = -1\,. \tag{6.8}$$

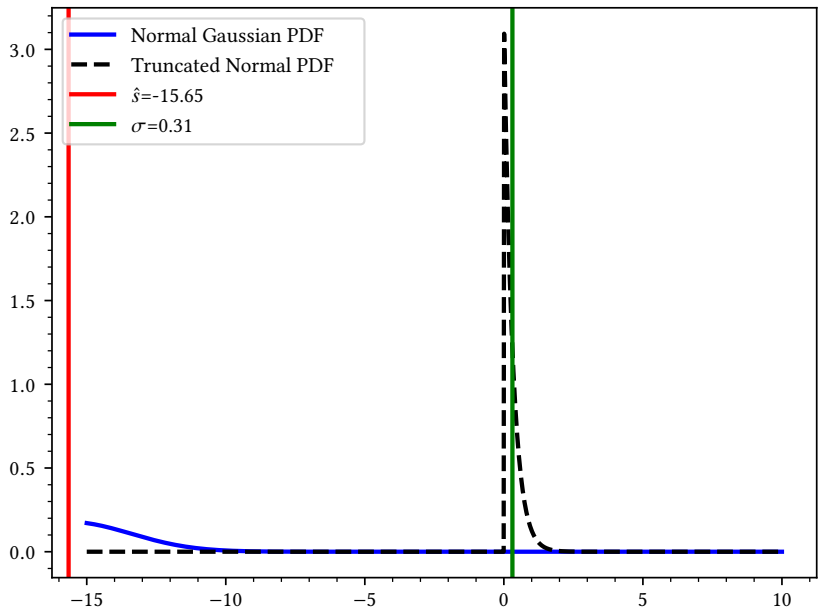

Figure 6.5: Truncated and Normal Gaussian PDF for $\xi = -7.0$

Such that the denominator in the hazard ratio,

$$\mathcal{H}(\xi) = \frac{\sqrt{\frac{2}{\pi}} e^{-\frac{1}{2}\xi^2}}{1 + \text{erf}\left(\frac{\xi}{\sqrt{2}}\right)},$$

quickly approaches zero as $\xi \to -\infty$. Due to this property of $\mathcal{H}$, a certain amount of care needs to be put into dealing with situations where a possibility of a division by zero can occur. A typical way to deal with these types of situations is to check the value of the denominator prior to the division. If its value is near or less than some tolerance, set it to some small tolerance level. This fix works in simple situations where the value of the numerator is not affected by the input variables. Unfortunately, the numerator of the hazard function changes quite significantly. Taking again the situation where $\xi \to -\infty$, while the denominator tends to zero the numerator also tends towards zero, such that is becomes sensitive to small changes in the denominator. Again it proves to be useful to plot the probability distribution function in order to develop an understanding as to the difficulties of the problem. Figure 6.5 illustrates the closure coefficients and the moments of the distribution for a case with a large negative ratio, ξ. In this case, the total number density and the variance of the Gaussian distributions are still set to the same values as presented in Figure 6.2 while the closure coefficient $\hat{s}$ is set to large negative value. The closure coefficients, $\hat{s}$ correspond to a normal Gaussian that is far to the left of the ξ axis and barely visible. As such the truncated distribution takes on the shape of a huge spike near zero. Additionally, the moment, σ, corresponding to the average surface area is near zero. In the limit where ξ tends towards

greater negative values the truncated normal distribution approaches a very large jump where the corresponding moment, σ would approach to zero. For these types of situations, it can be rather difficult to evaluate to high-accuracy with finite machine precision as in the case of the PGM the average particle surface, σ would be zero. Having the moment, σ result in zero would disrupt the stability of the PGM. In this situation, the denominator in the $\mathcal{H}$ function is extremely close to zero but, due to finite precision present in numerical computation, computation of $\mathcal{H}$ in its limit often returns a division by zero. The numerical error thus generated from computing $\mathcal{H}$ can be interpreted as situations where the PGM, while having valid and realizable closure coefficients, results in moments that are near zero yet still play a significant impact in the resulting statistics of the system. This relationship can also be extended to the surface-weighted moments, $\dot{\sigma}$ and $\dot{\Psi}_{ss}$ such that for a given set of valid closure coefficients the weighted moments might be near zero and numerically difficult to evaluate without significant numerical error.

From practical experience, the difficulties of computing $\mathcal{H}$ occurs at around $\xi \lessapprox -6.0$. Furthermore, while it does appear in Figure 6.4 that the hazard ratio reaches a linear function in its limit as $\xi \to -\infty$ this is not the case. It can be shown that the Mills ratio is strictly convex and reaches an asymptotic expansion in its limit such that given the Mills ratio,

$$m(\xi) = \frac{1 - \Phi(\xi)}{\phi(\xi)}, \tag{6.9}$$

$$m(\xi) \approx \frac{1}{\xi} - \frac{1}{\xi^3} + \frac{1 \cdot 3}{\xi^5} - \frac{1 \cdot 3 \cdot 5}{\xi^7} + \dots, \quad \text{for} \quad \xi \to \infty, \tag{6.10}$$

Eq. (6.10) hold true [21, 26, 7, 1, 4, 25]. As the Mils ratio, or the Hazard function, can be difficult to evaluate past $\xi = -6$ this asymptotic limit could be used in order to approximate the hazard function as $\xi \to -\infty$. While the relative error between the computed hazard function and its asymptotic expansion may prove to be quite low and in the range of $1 \times 10^{-7} - 1 \times 10^{-5}$ in many cases, there is a region between $\xi \approx [-3, -100]$ where the relative error produced between the asymptotic expansion and its true value computed with a high degree of numerical precision is significant, such that it would cause unacceptable errors in the PGM. In other words during the process of converting from the closure coefficients to the moment variables, if one uses the asymptotic expansion in order to circumvent the numerical error obtained in computing $\mathcal{H}$, one finds situations where the computed moment variables admit non-physically possible values. For instance the moments corresponding to the average particle surface, σ or $\dot{\sigma}$, return values that are less than zero. Furthermore, the use of an approximation for $\mathcal{H}$ have other significant cascading effects on the numerics of the system. Since the PGM is constructed from a set of coupled closure coefficients, small errors in the evaluation of the moments from the closure coefficients or evaluation of the closure coefficients from the moments has wide sweeping effects on the stability of the PGM. For instance, a key feature of the PGM is the positive-definiteness of the system and while it has been shown in Section 4.2.5 that this can be guaranteed for our set of weights, numerical rounding error in the approximation of $\mathcal{H}$ quickly results in the matrix shown in Eq. (4.46) to have negative eigenvalues, disrupting the stability of the PGM. Many other numerical approx-

imations and bounding functions of the Mills function exist and have been tried but still results in significant relative numerical error when computing moments of the PGM from the closure coefficients.

6.1.2 Scaled Complementary Error Function

As discussed above, the difficulties of converting the closure coefficients to moment variables of the PGM or *vice versa* has to do with the numerical error generated in the evaluation of $\mathcal{H}$ for large negative values of ξ. Again the function that is difficult to compute is

$$\mathcal{H}(\xi) = \frac{\sqrt{\frac{2}{\pi}} e^{-\frac{1}{2}\xi^2}}{1 + \operatorname{erf}\left(\frac{\xi}{\sqrt{2}}\right)} .$$

This function can be rather difficult to compute accurately using finite precision arithmetic as numerical error occurs in the denominator of $\mathcal{H}$. Thankfully, this situation has already been encountered and a function called the scaled complementary error function, erfcx, has been developed especially for this type of situation, situations where large values of a normal Gaussian in conjunction to the error function are required. The scaled complementary error function, erfcx is often expressed as,

$$\operatorname{erfcx} x = e^{\xi^2} \operatorname{erfc} \xi , \tag{6.11}$$

where erfc is the complimentary error function,

$$\operatorname{erfc}(\xi) = 1 - \operatorname{erf}(\xi) . \tag{6.12}$$

As the error function is a odd function

$$\operatorname{erf} \xi = - \operatorname{erf} (-\xi) , \tag{6.13}$$

$\mathcal{H}$ can be expressed with the use of the scaled complementary error function,

$$\mathcal{H}(\xi) = \frac{\sqrt{\frac{2}{\pi}}}{\operatorname{erfcx} (-\frac{\xi}{\sqrt{2}})} . \tag{6.14}$$

The numerical implementation for the evaluation of the scaled error function that has been used in this work is the implementation by S. G. Jonson [23]. This implementation is based on the computation of the Feddeyeva and Voigt functions along with a Chebyshev polynomial approximation in order to accurately and with relatively low computational cost compute the complementary error function to sufficient accuracy with finite machine precision [8, 22, 32, 23]. The relative error from using erfcx when compared to a high-precision solver has been cited to be better than 1×10^{-13} [23]. The scaled complementary error function has been implemented and is called anytime evaluation of $\mathcal{H}$ is required. In practice it can be shown that conversion of the

moments of the PGM remains stable for most values of $\xi \gtrapprox -100$. At this point one would assume that the numerical error in computing the moments of the PGM are now due to the fact that the resulting moments, such as the average surface, σ are near-zero. This numerical error can be easily handled by developing a state that would effectively act as a near-zero state of the flow. The implementation and discussion of these near-zero states are explored in Section 7.3.

6.1.3 Conversion from Moments to Closure Coefficients

As the PGM has been implement with surface-weighted statistics the conversion from the moment variables to the closure coefficients is expressed as the following coupled set of equations,

$$\dot{\sigma} = \sqrt{r_{ss}} \left(\xi + \frac{1}{\xi + \mathcal{H}} \right) , \tag{6.15}$$

$$\dot{\Psi}_{ss} = r_{ss} + \frac{r_{ss} \left(\mathcal{H} \left(\xi + \mathcal{H} \right) - 1 \right)}{\left(\xi + \mathcal{H} \right)^2} , \tag{6.16}$$

with again ξ being the ratio of the closure coefficients corresponding to the particle surface, $\xi = \dot{s}/\sqrt{r_{ss}}$. Lucky these coupled set of equations can be regrouped into a single expression,

$$\frac{\dot{\sigma}^2}{\Psi_{ss}} = f(\xi) = \frac{\left(1 + \xi^2 + \xi \mathcal{H} \right)^2}{3\xi\mathcal{H} + 2\mathcal{H}^2 + \xi^2 - 1} . \tag{6.17}$$

As the derivatives of the hazard ratio can be expressed in closed form,

$$\frac{\mathrm{d}\mathcal{H}}{\mathrm{d}\xi} = -\mathcal{H} \left(\xi + \mathcal{H} \right) , \tag{6.18}$$

and it is known that the Mills ratio is a strictly convex function [25] a simplified Newton-Raphson method can be used in order to efficiently solve the non-linear system, Eq. (6.17), for a given ratio of weighted moments, $\dot{\sigma}$ and $\dot{\Psi}_{ss}$. As shown in Figure 6.6, this function is very well behaved such that solving for any value with positive x can be done in very few iteration. While solving for values much less than -10 can be difficult due to the "flatness" of the curve as this function is convex using a Newton-Raphson method with adequate convergence criteria should be sufficient for any practical and physically meaningful state of the PGM.

6.2 Numerical Methods, Space-Homogeneous Case

Numerical results of space-homogeneous cases for the PGM are significantly less expensive to obtain when compared to three-dimensional cases. This is because in a space-homogeneous case the coupled set of governing PDEs of the PGM, Eqs. (4.38)–(4.43) as shown in Section 4.4 can be simplified in both the original log-diameter based PGM and the surface-based PGM. As such a robust stiff ordinary differential equation solver was used to obtain solutions of the log-diameter

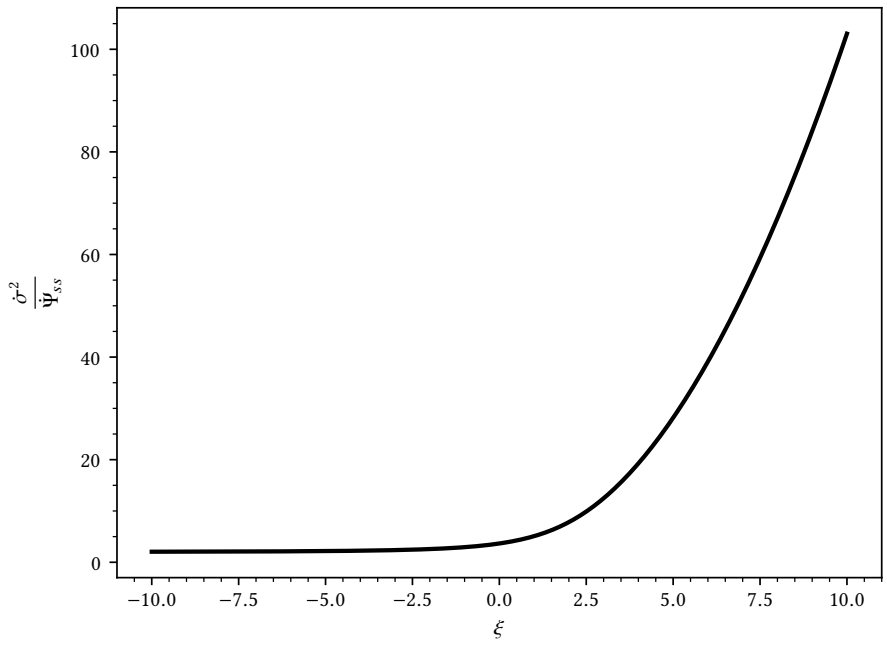

Figure 6.6: Ratio of $\frac{\dot{\sigma}^2}{\dot{\Psi}_{ss}}$ for given ξ

and surface-based PGM [29]. The kinetic solution used to compare and validate the results are obtained via the implementation of the Efficient Kinetic Solver as outlined in Section 5.

6.3 Numerical Methods, Three-Dimensional Case

Calculations are done using a simple first-order finite-volume scheme using the Harten-Lax-van Leer (HLL) flux function [11]. A simple first order accurate point-implicit time-marching scheme is used that treats the fluxes explicitly, while treating the local sources implicitly. This is necessary, as the source terms can often be stiff. Fortunately, as the sources take on simple expressions, this can be done quite easily. The previously shown balance law, Eq. (4.11) can be expressed in a discrete form,

$$\bar{\boldsymbol{U}}_i^{n+1} = \bar{\boldsymbol{U}}^n + \frac{\Delta t}{V_i} \sum_{j=0}^{\text{faces}} \boldsymbol{F}_j \cdot \hat{n}_j A_j + \Delta t \bar{\boldsymbol{S}}^{n+1} \,. \tag{6.19}$$

In a three dimensional case, each cell in the domain has a volume such that in Eq. (6.19), V_i, is the volume of cell i. The bar notation is used for the solution vector, $\boldsymbol{U}$, flux vector, $\boldsymbol{F}$, and the source vector, $\boldsymbol{S}$, in order to represent the cell average value. In this work an explicit-Euler time-marching method is implemented such that in Eq. (6.19), $\bar{\boldsymbol{U}}_i^n$, is the average cell solution in cell i, at the current time step and, $\bar{\boldsymbol{U}}_i^{n+1}$, is the average cell solution at the next time step. Numerical fluxes, $\boldsymbol{F}_j$, are computed between each cell surface, A_j, using the HLL flux function. Finally, as previously mentioned as the source term can be stiff the numerical evaluation of the source vector is done implicitly. For lower-order moment-based methods, the wavespeeds of the

systems are known. Unfortunately for the surface-based PGM these can be shown to be quite difficult to obtain in closed form. As such the flux Jacobian is constructed analytically where its eigenvalues are numerically computed via means of algorithmic differentiation.

Chapter 7

Numerical Results

This chapter demonstrates the capabilities of the PGM by first presenting a space-homogeneous case and it's agreement with the known steady-state solution. The presented space-homogeneous case is first presented with a simplified source term as presented in Section 4.3. A case without evaporation is evaluated as to be compared with the exact kinetic solution in addition to the previously described log-diameter based PGM. Furthermore a space-homogeneous case with evaporation is then considered in order to demonstrate the capabilities of the surface-base PGM. Finally a three-dimensional case is presented for a "puff" of particles in order to observe the settling of particles in three-dimensional space.

7.1 Space-Homogeneous Case

In order to validate the model, a simple space-homogeneous case is used to compare the results obtained from the PGM with the known solution obtained by solving the kinetic equations, Eq. (4.3), directly using a forth-order Runge-Kutta method in addition to also comparing the results obtained with the original log-diameter based PGM. For this case, the initial conditions are chosen to be described by a surface-area-based distribution function with moments given in Table 7.1a. A cloud of particles has an initial downward (positive x in this case) velocity that is far higher than the terminal velocity. The particle cloud therefore decelerates to its steady state settling configuration. The particles are modelled as being droplets of water in the medium of air such that the density of the particles and of the background are given by $\rho_p = 1000\,\mathrm{kg\,m^{-3}}$, and $\rho_f = 1.225\,\mathrm{kg\,m^{-3}}$, respectively. The dynamic viscosity of air is set as $\mu_f = 1.82 \times 10^{-5}\,\mathrm{kg\,m^{-1}\,s^{-1}}$, which corresponds to ambient air at 20 °C. This leads to source-term parameters, $\gamma = 971\,641\,\mathrm{s\,m^{-2}}$ and $\phi_x = 9.79\,\mathrm{m\,s^{-2}}$, for a simplified expressions in the source term.

7.1.1 Space-Homogeneous Case Without Evaporation

Both the surface-weighted PGM and the original log-normal PGM are investigated. In order to set initial conditions for the log-normal variant of the model, classical moments based on the

Table 7.1: Initial conditions for space-homogeneous particle-settling case

(a) Surface-weighted moments

Moment	Initial value
$\dot{n}$	1
$\dot{\mu}_i$	$10\,\mathrm{m\,s^{-1}}$
$\dot{\Theta}_{ij}$	$(1\,\mathrm{m^2\,s^{-2}})\delta_{ij}$
$\dot{\sigma}$	$5.6 \times 10^{-7}\,\mathrm{m^2}$
$\dot{\Psi}_{is}$	$0\,\mathrm{m^3\,s^{-1}}$
$\dot{\Psi}_{ss}$	$8.58 \times 10^{-14}\,\mathrm{m^4}$

(b) Traditional moments

Moment	Initial value
n	1
μ_i	$10\,\mathrm{m\,s^{-1}}$
Θ_{ij}	$(1\,\mathrm{m^2\,s^{-2}})\delta_{ij}$
$\bar{\zeta}$	-8.11
Ψ_{id}	$0\,\mathrm{m\,s^{-1}}$
Ψ_{dd}	0.113

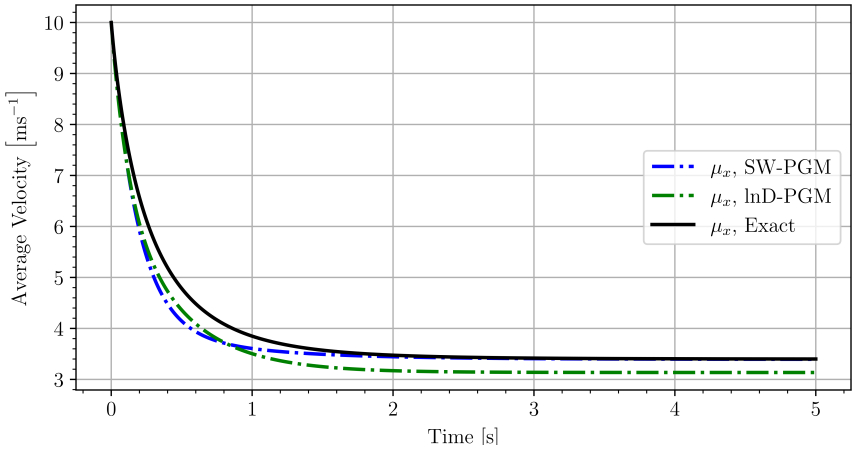

Figure 7.1: Surface-weighted average particle velocity obtained from model and Lagrangian solver.

logarithm of particle diameter must be evaluated for the initial condition. The values obtained are shown in Table 7.1b. These serve as the initial conditions for the log-normal PGM computation.

The results obtained from the simplified ODEs are compared to an implementation of the kinetic solver, as presented in Section 5. In Figure 7.1, one can observe that the model closely follows the Lagrangian solution, while the variance shown in Figure 7.2, and the covariance, Figure 7.3, overshoots the solution. Despite overshooting the transient solution all quantities recover the exact steady-state solution. Looking at Figure 7.3, one can observe a positive covariance during the time scale, which implies that smaller particles are decelerating faster than the larger particles. This is due to the fact that the particles start with a large initial velocity of $10\,\mathrm{m\,s^{-1}}$, as such the larger particles take much longer to reach their terminal velocity whereas the smaller particles are slowed down much faster due to their lower initial momentum. The variance of the particle velocity can also be observed in Figure 7.2. Here, the variance, $\dot{\Psi}_{xx}$ quickly increases as the smaller particles slow down, indicating a strong coupling with the velocity. Furthermore, the initial large positive variance in velocity indicates a strong coupling of the particles velocity with respect to the average velocity. The variance is originally over predicted but finally relaxes to the correct value. In addition the viewing the evolution of the moments, these moments can be

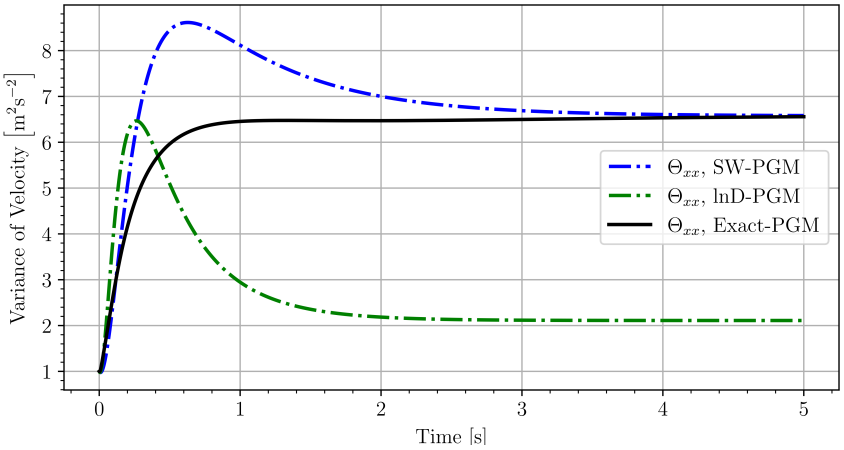

Figure 7.2: Surface-weighted velocity variance obtained from model and Lagrangian solver.

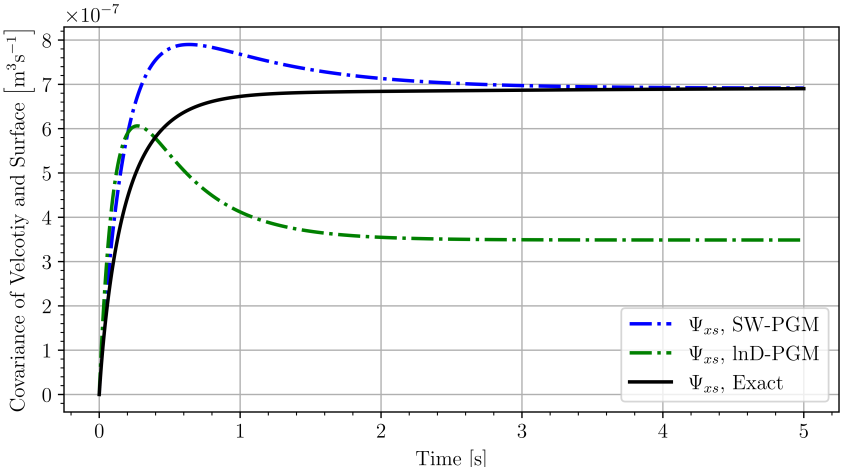

Figure 7.3: Surface-weighted velocity covariance obtained from model and Lagrangian solver.

translated to the closure coefficients of the distribution function, this can in turn be mapped to the predicted form of the distribution itself, Eq. (4.45).

Figure 7.4a illustrates the initial distribution, $\mathcal{F}$, for the current space-homogeneous case. One can observe the initial distribution presented in this figure takes the form of a multivariate Gaussian without covariance, as per the initial conditions of this space-homogeneous case. The exact steady-state solution has also been included for the polydisperse flow. The steady-state solution takes the form of a line, such that each particle, depending on its surface, has a predetermined terminal velocity. From the steady-state solution, Eq. (4.94), one can observe that particles with a greater surface area arrive at a larger terminal velocity. Furthermore, at around $t \approx 1.0\,\text{s}$, the region where both the variance and covariance overshoot the solution the same effect can be observed in the distribution function, Figure 7.4e. At this time the lower tail of the distribution overshoots the steady-state solution but as time increases, the distribution fully collapse onto the correct steady-state solution.

In addition to the evolution of the distribution function one can compare it to the previous PGM model. Note that, in this case, it is difficult to have an analogous comparison to both models since the probability density function for the PGM using surfaced-based statistics cannot admit the same shape as the probability density function for log-normal diameter-based statistics. For this simple space-homogeneous case the properties of the particles and the fluid medium remain the same. Furthermore, a translation between surfaced-based moments of the PGM to their corresponding log-diameter based statistics of the previous PGM can be derived. The moments can be obtained by evaluation of the moments of the diameter-based distribution, $\mathcal{F}_D$ with the appropriate surface-based weighted statistics such that,

$$n\sigma = \langle s\mathcal{F}_D \rangle \ , \tag{7.1}$$

$$\sigma = \pi \exp\left[2\mu_d + 2\Psi_{dd}\right] \ , \tag{7.2}$$

and

$$n\Psi_{ss} = \left\langle (s-\sigma)^2 \mathcal{F}_D \right\rangle \ , \tag{7.3}$$

$$\Psi_{ss} = \pi^2\sigma^2 \left(\exp\left[4\Psi_{dd}\right] - 1\right) \ . \tag{7.4}$$

In Eqs. (7.1)–(7.3), the corresponding log-normal average particle diameter, μ_d can be related to the average particle surface, σ and the log-normal variance of the particle diameter, Ψ_{dd} can be related to the variance of the particle surface, Ψ_{ss}. Figures 7.1–7.3 also show the evolution of the PGM using diameter-based statistics for the same initial conditions to those presented in the surface-weighted PGM. The illustrated correct steady-state solution, Eq. (4.94), for the particles given their initial conditions is also presented. In Figure 7.4b, one can notice that the initial distribution, much like the surface-weighted PGM model, takes on a form of a Gaussian without any covariance. The Gaussian for this case is stretched in the surface space as the expression for the probability density function, $\mathcal{F}_D$, is a function of the log-normal of the particle diameter. As time progresses the distribution takes on a curve such that it is never able to rest onto the

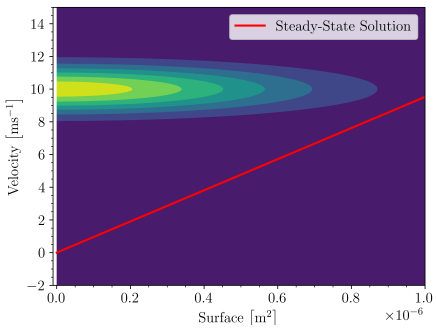

(a) SW-PGM, $t = 0$ s

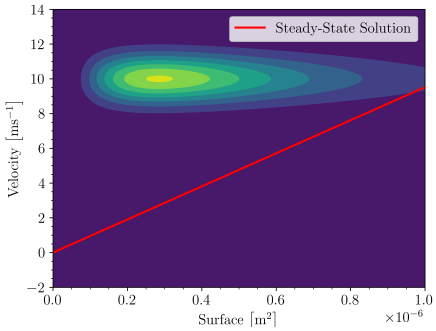

(b) Log-normal PGM, $t = 0$ s

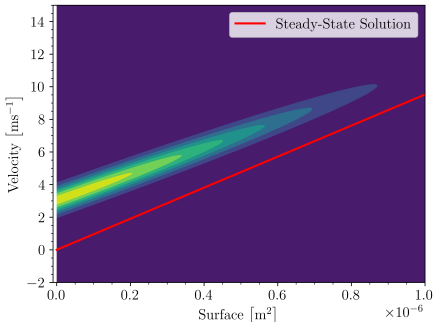

(c) SW-PGM, $t = 0.2$ s

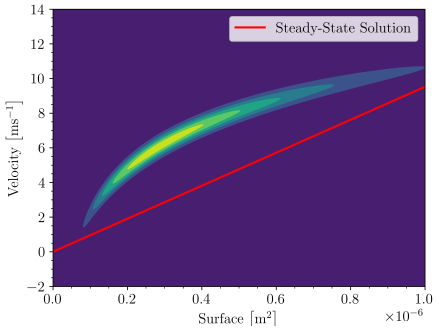

(d) Log-normal PGM, $t = 0.2$ s

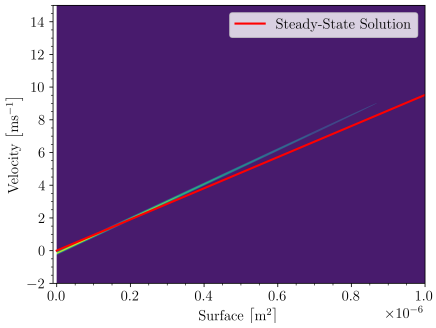

(e) SW-PGM, $t = 1.0$ s

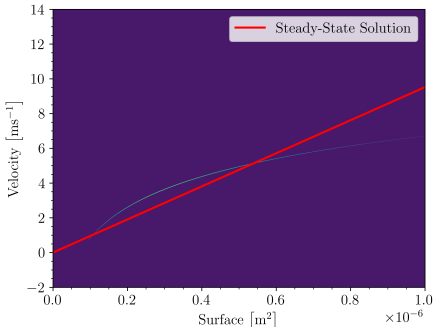

(f) Log-normal PGM, $t = 1.0$ s

Figure 7.4: Distribution function for a settling cloud of particles subjected to gravity, buoyancy, and Stokes drag as compared to the correct terminal velocity line: surface-weighted PGM and original log-normal PGM.

steady-state solution. In its limit the set of coupled ODEs for the space-homogeneous case, using log-diameter-based statistics settles along the log-diameter of the particles, Eq. (4.95). In certain cases, namely in a mono-disperse flows or situations where the spread of particle size is relatively small, the curved nature of the distribution, $\mathcal{F}_D$ would only slightly impact the deviation from the exact solution. Unfortunately, in more practical cases, as the log-diameter PGM is unable to recover the settling of particles the relaxation parameter, $\tau_{\mathcal{G}}$ has to be tuned in order to obtain results that follow closer to the known exact solution to the kinetic equations [5].

7.1.2 Space-Homogeneous Case With Evaporation

The following space-homogeneous case with evaporation has almost similar initial conditions to the the space-homogeneous case without evaporation. In this case, the key difference is the addition of particle evaporation. The use of an evaporation constant has for effect of altering the source term vector, $\boldsymbol{S}$. The evaporation constant, α, was selected in order to properly capture the effect the evaporation rate has on the moments of the model. Over the time range of

$$t = [0.0\,\mathrm{s} - 5.0\,\mathrm{s}] \tag{7.5}$$

setting the evaporation as

$$\alpha = 1 \times 10^{-7}\,\mathrm{m^2\,s^{-1}}, \tag{7.6}$$

is such that particle evaporation is fast enough to be observed during the time interval, yet slow enough that a significant amount of particles remain at the end of the 5.0 s interval. Much like the previously shown space-homogeneous case the evolution of the moments can be plotted over time. In addition to the moments related to the particle velocity, $\dot{\mu}_x$, $\dot{\Theta}_{xx}$, $\dot{\Psi}_{xs}$, the time evolution of the previously time-invariant moments of the case without evaporation can also be plotted. As this case has the added evaporation in the source term there is not the presence of any time-invariant moments. In addition to the weighted moments that were shown in the space-homogeneous case without evaporation, the non-weighted moments along with their respective closure coefficients can also be plotted over time. Furthermore, the kinetic solver, as presented in Section 5, can be leverage to compare the results obtained from PGM to the known kinetic solution. To begin, Figure 7.5 very closely resemble the ones presented in the space-homogeneous without evaporation. The main difference being that at approximately $t = 0.5\,\mathrm{s}$ the exist a noticeable bump that is present in both the particles variance of velocity and covariance with respect to size. In the case without evaporation, Figures 7.2–7.3, the results are a lot less spread out when compared to the case with evaporation. As the particles are slowly evaporating away, such that the average particle size is decreasing, this has for effect of altering their velocity due to the drag forces being proportional to the size of the particles. As such, one can notice that the obtained moments, namely those obtained from the variance of velocity and covariance of velocity with surface area, follow much closer to the exact kinetic equation. Comparing the space-homogeneous case with evaporation to the one without, the average particle velocity both follow the exact solution over its evolution to significant accuracy. What is gained in the case

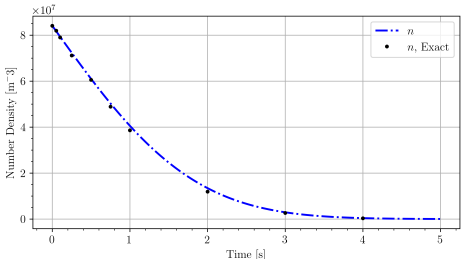

(a) Number density obtained from model and Lagrangian solver

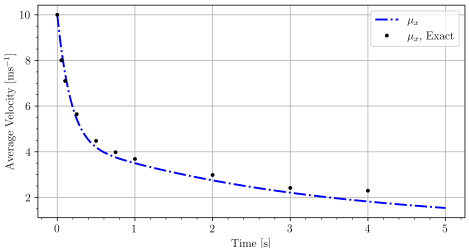

(b) Average particle velocity obtained from model and Lagrangian solver

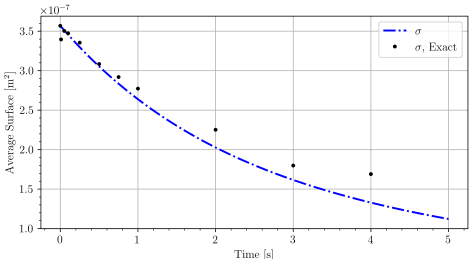

(c) Average particle surface obtained from model and Lagrangian solver

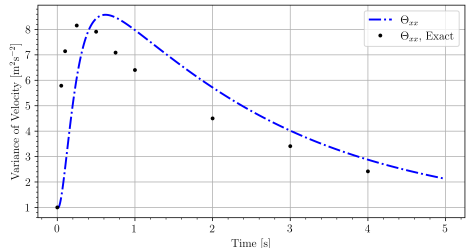

(d) Variance of particle velocity density obtained from model and Lagrangian solver

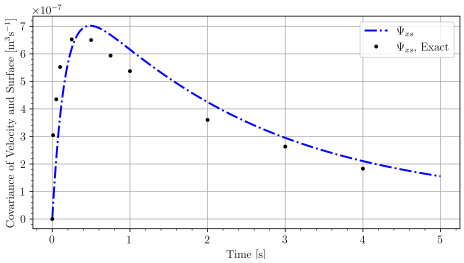

(e) Covariance of particle velocity and surface obtained from model and Lagrangian solver

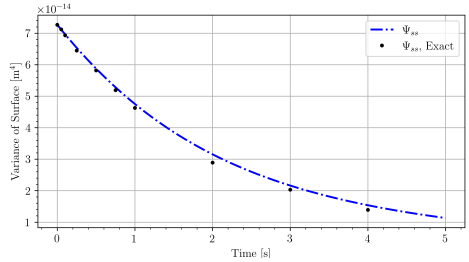

(f) Variance of particle surface obtained from model and Lagrangian solver

Figure 7.5: Moments obtained from model and Lagrangian solver for a space-homogeneous case with evaporation

with evaporation are the moments, Θ_{xx} and Ψ_{xs} following more closely the exact kinetic solution during their evolution. The remaining moments, n, σ and Ψ_{ss} are directly related to the number of particles in the system and their size. As these two factors are continuously changing in the system due to evaporation affecting the size of the particles and the total number of particles in the system as particles are "evaporating away". It can be useful, similar to the other moments obtained by the PGM, to then compare them to the kinetic solution obtained by the Lagrangian solver. To begin, the number density of the particles in the system, Figure 7.5a, is decreasing over the time interval. This is expected as all the particles, due to evaporation, have a decreasing surface area. For particles with a very small surface area, this means they become even smaller at which point they eventually become so small that they effectively disappear in the system. This would explain the total number density of the particles in the system decreasing over the time interval. One would expect that over a longer time interval this total number density would eventually reach zero such that all the particles in the system have evaporated away. The governing equation for the rate of particle evaporation, Eq. (2.6) is directly proportional to the current area of the particles such that the larger particles are more significantly affected by the rate of evaporation than the smaller ones. This relationship explains the initial sharp decrease in the number density of the particles in the system, then towards the end of the observed time interval when only smaller particles are remaining in the system the particles in the system are evaporating at a much slower rate. Additionally, as the particles surface area are constantly decreasing due to evaporation it is expected that the average particle surface is also decreasing and can be shown to very closely resemble the exact kinetic solution as shown in Figure 7.5c. What is more of interest is the variance of the particles surface area, Ψ_{ss}. This variance, representing the spread of the particles surface area in the system is also decreasing. This property can also be explained by the evaporation of the particles in the system. As per the initial conditions, the particles in the system start with an initial range of surface area, Ψ_{ss}. Such that the initial particle surface area is a normal Gaussian distribution with average surface area, σ with a variance of Ψ_{ss}. As particles in the system are evaporating away at a rate that is proportional to their size it is expected that the distribution of this size does not remain constant. Moreover, one can notice a decrease in variance of the particles surface area, Figure 7.5f. This decrease in variance indicates that the particles surface area is more tightly coupled to its average surface area, σ. One can interpret this decrease in variance of size in the following manner. During the evaporating process the average surface area of all the particles in the system are decreasing but additionally the spread of such particles becomes smaller, such that further along in the time interval the spread of particle surface area is much closer to the ever decreasing average area. These additional moments, when compared to the exact kinetic solution follow very closely the evolution over the entire time interval.

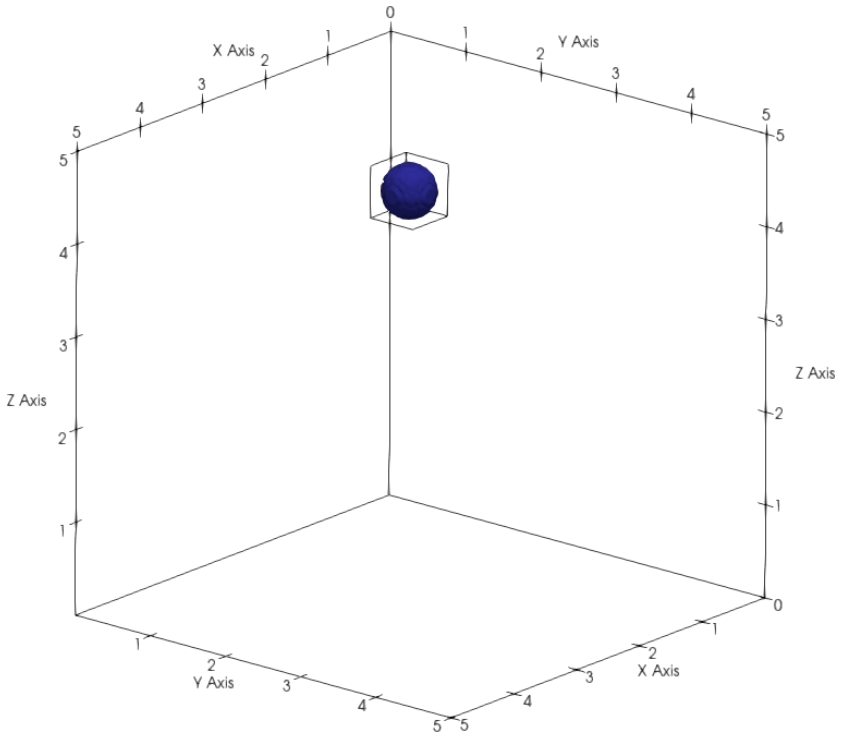

Figure 7.6: Initial condition for a puff of polydisperse particles with an initial x-direction bulk velocity with a cross wind in the y directions. Region where $n \geq 1 \times 10^3$ particles/m^3 is visualized.

7.2 A Three-Dimensional Case

As a final demonstration case to show how the direct tracking of higher-order particle statistics yields information that is often invisible to traditional methods, a puff of particles with initial velocity moving and settling in a background cross wind is considered. The domain of this problem is a cube with five-meter sides. The puff is initially positioned at (x, y, z) coordinates of (1 m, 1 m, 4 m) and has a diameter of 0.5 m. The particles for this case are assumed to follow a log-normal distribution of diameters. The original log-normal version of the PGM is considered first. Within the initial sphere of particles, the particle number density is $n = 29.6 \times 10^6$ particles/m^3. The mean surface area of the particles is $\sigma = 4.04 \times 10^{-6}$ m^2, with variance, Ψ_{ss} of 6.21×10^{-12} m^4. The initial velocity is 3 m s^{-1} in the x direction with a variance of 0.1 m s^{-2} in all directions. All covariances are initially zero. The background wind is 1 m s^{-1} in the positive y direction. Particle properties are chosen such that the initial value of $\tau_{\mathcal{G}} = 0.1$ s. This allows all relevant physical processes to act on similar time scales. The initial condition is illustrated in Figure 7.6.

The domain is discretized using 4,096,000 cells, and time steps are limited by the maximum wave speed within the domain at every step with a CFL number of 0.15.

For this case, results are visualized at $t = 0.5$ s and $t = 1$ s. Figure 7.7 shows the predicted average particle diameter at these two times. Regions where the number density of particles is

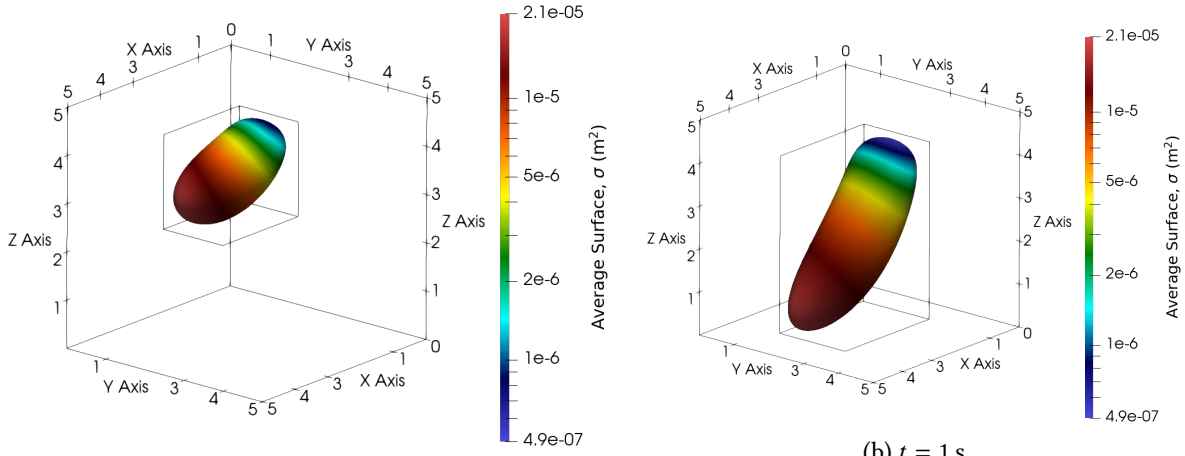

(a) $t = 0.5\,\mathrm{s}$ (b) $t = 1\,\mathrm{s}$

Figure 7.7: Particle size distribution. Region where $n \geq 1 \times 10^3$ particles/m^3 is visualized.

larger than 1×10^3 particles/m^3 are visualized. One can clearly observe that the large particles have kept their initial velocity for longer, as they are less affected by particle drag. They have also been more heavily affected by gravity. This is why the larger particles have travelled farther in the x direction and fallen further. The smaller particles decelerated due to drag much more quickly and have a lower terminal velocity. They are also more strongly affected by the drag of the background wind. These effects cause a cloud of smaller particles to remain higher in the domain while translating more in the y direction due to the wind.

The importance of the covariance between particle sizes and velocities is shown in Figures 7.8 and 7.9. Figure 7.8 examines the bulk vertical velocity and its covariance with particle size. In the left subfigures, one can clearly see that the particles that have fallen furthest have the most negative vertical velocity, obviously. More importantly, the right subfigures show that the covariance between the vertical component of the velocity and the particle size is always negative and has the highest magnitude in the particles that have fallen furthest. A negative covariance indicates that particles with largest negative vertical velocities are more likely to be larger particles. Again, this is entirely expected, however it is an effect that is not often directly considered by classical models. It is expected that this information will lead to improved predictive capabilities for the PGM models.

Figure 7.9 shows statistics related to the x-direction velocity. The left-hand subfigures show the x component of the bulk velocity. One can see that, at $t = 0.5\,\mathrm{s}$, the particles moving the fastest in this direction have a velocity of about $3\,\mathrm{m\,s^{-1}}$, which was the initial value. This is because there is a group of larger particles that has not yet been significantly slowed by drag and has travelled the largest distance in this direction. This is confirmed by examining the plots on the right, which show the covariance between the x component of velocity and the particle size. The positive value of this moment indicates that larger particles are more likely to have larger positive x-direction velocities. One can also observer that, by $t = 1\,\mathrm{s}$, drag forces have begun to have more of an effect on particles of all sizes. The average x-direction velocities are decreasing, as is the covariance.

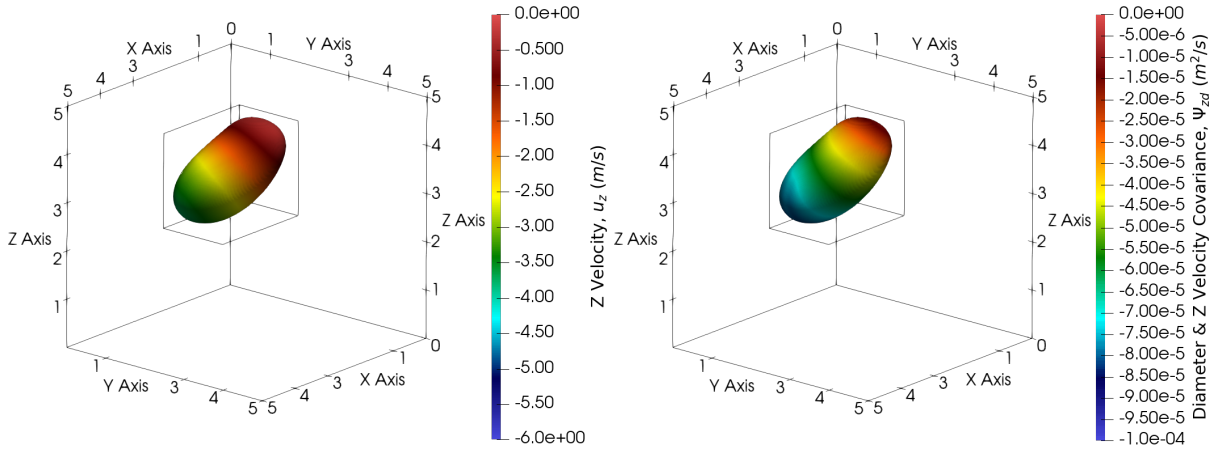

(a) μ_z, $t = 0.5$ s (b) Ψ_{zd}, $t = 0.5$ s

(c) μ_z, $t = 1$ s (d) Ψ_{zd}, $t = 1$ s

Figure 7.8: z-direction bulk velocity and covariance with particle size. Region where $n \geq 1 \times 10^3$ particles/m^3 is visualized.

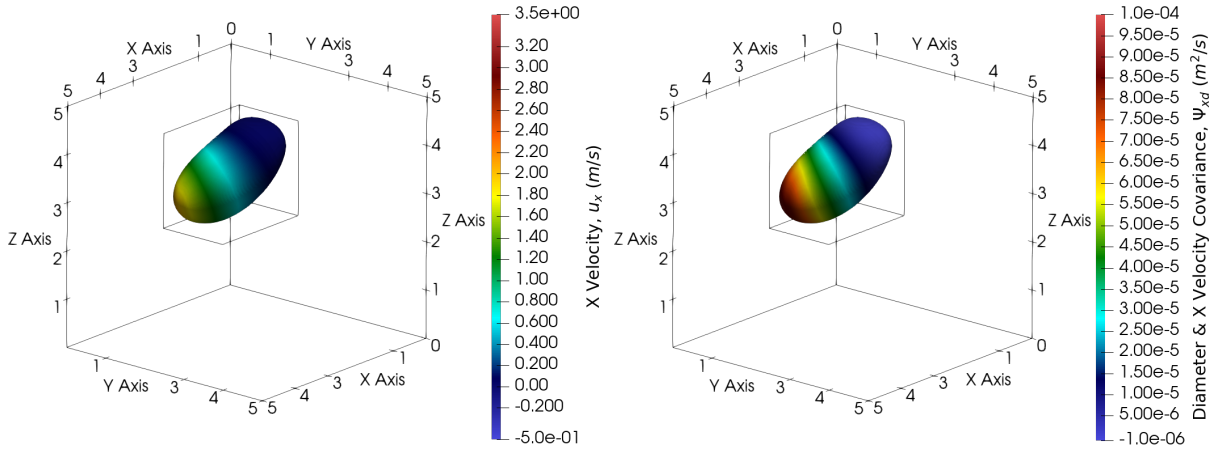

(a) μ_x, $t = 0.5$ s

(b) Ψ_{xd}, $t = 0.5$ s

(c) μ_x, $t = 1$ s

(d) Ψ_{xd}, $t = 1$ s

Figure 7.9: x-direction bulk velocity and covariance with particle size. Region where $n \geq 1 \times 10^3$ particles/m^3 is visualized.

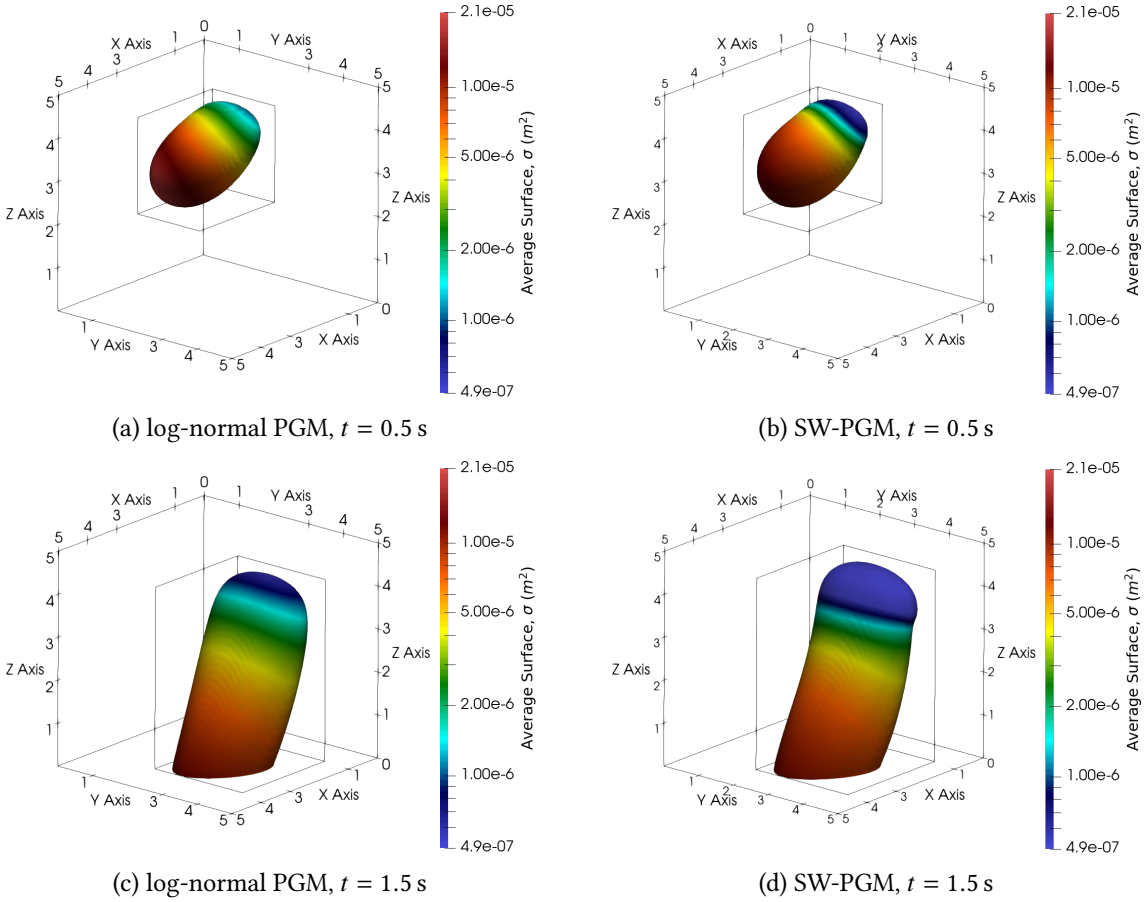

(a) log-normal PGM, $t = 0.5$ s

(b) SW-PGM, $t = 0.5$ s

(c) log-normal PGM, $t = 1.5$ s

(d) SW-PGM, $t = 1.5$ s

Figure 7.10: Particle size distribution as predicted by the log-normal and surface weighted versions of the PGM. Region where $n \geq 1 \times 10^3$ particles/m^3 is visualized.

7.2.1 Comparison with prediction of the surface-weighted PGM

As a final study, differences in the predicted solution for this problem provided by the original log-normal PGM and the new surface-weighted PGM are explored. Figure 7.10 compares the local particle-size distribution for this case as predicted by each model results are visualized at $t = 0.5$ s and $t = 1.5$ s. The left-hand subfigures were obtained from the log-normal PGM, which the right-hand figures used the surface-weighted PGM. For this case, differences are surprisingly minor. The exact shape of the region occupied by particles is slightly different and the distribution of particle sizes is not quite identical, however results are very close. The similarity of the two predictions is probably due to the fact that the variance in particle size is not overly large in this case. It is expected that larger differences in predictions should be expected for polydisperse flows that display a larger range of particle sizes.

7.3 Realizable States of the PGM and Numerical Difficulties

While the mathematics behind of the implementation of the PGM remains very similar from the space-homogeneous case when compared to the three-dimensional case many numerically

difficulties appear when the PGM is implemented in a higher-dimensional case. As previously mentioned, one of the main difficulties in the PGM is the translation from moment variables to the closure coefficients and *vice versa*. In the space-homogeneous case without evaporation this need of translation is not a significant issue as the time invariant variables, $\dot{n}$, $\dot{\sigma}$ and $\dot{\Psi}_{ss}$ are such that a translation between the moment variables and closures coefficients can be done trivially and to high precision. Furthermore, numerical error that might appear during the computation of the moment variables from the closure coefficient does not become an issue as the $\mathcal{H}$ function only needs to be computed once at the start of the simulation. This also has for an added benefit that, during the time interval, there are not any significant compounding numerical error generated during the translation of moment variables to closure coefficients. On the other hand, in the three-dimensional case this step, using the Newton-Raphson method to solve for the closure coefficients then using the obtained $\mathcal{H}$ function in conjunction with the scaled complementary error function needs to be preformed at each time step for each cell in the domain. Even with the implementation of the scaled complementary error function it is still possible that the computation predicts a non-realizable state. As these calculations are preformed many times for situations with very refined meshes, small numerical errors can propagate in the system and result in mathematical artifacts or, more importantly, lead to a non-realizable state of the PGM. These non-realizable states often result in numerical computation crashing and can be very difficult to manage due to complexity of initial states that might eventually lead to non-realizable states such as those created due to numerical underflow in computation of the moments. Some of these non-realizable states can be obvious to spot but rather complex to fix. For instance, due to the physics of the problem and the mathematical nature of the moments in the PGM it is mathematically impossible to obtain a negative average surface and weighted average surface, σ, $\dot{\sigma}$. Furthermore, the variance of the particles surface area, Ψ_{ss}, $\dot{\Psi}_{ss}$ has to also always admit a positive value. Furthermore, it is also self evident that the PGM cannot admit a negative number density, n and $\dot{n}$. While these values can be very near zero and zero in its limit, it should be physically impossible to reach such states. Unfortunately due to many compounding effects such as those previously mentioned, the PGM without any check often arrives at these non-realizable states.

In order to improve the robustness of the implementation of the PGM in three-dimensions, checks can be preformed to verify if the PGM has arrived at a non-realizable state. If a non-realizable state has been detected in the domain that cell can be flagged and altered such that its values are similar to the non-realizable values yet the cell would be now considered at a realizable state of the PGM. A simple example of this would be if the number density is a small negative number, as it is known the number density cannot be a negative number it is more-likely that the "true value" of this state is either zero or near-zero. As such, altering the number density to a small near-zero value would be a possible fix to this situation. While these states can be rather trivial in most situations to check, correcting a non-realizable state can be significantly more difficult to preform correctly without introducing additional error in evaulation of the moments. The approach that was taken in this implementation works in the following manner. Initially at each time step all the cells in the PGM are checked to see if they admit a non-realizable state. This

check is preformed in two parts, the first part is used in-order to quickly check if the required positive moments in the system are indeed positive. This is done rather simply by verifying if the number density, and the surface related moments ($\dot{n}$, $\dot{\sigma}$, $\dot{\Psi}_{ss}$) are above a set tolerance. If such values are under a predefined tolerance its "true values" are assumed to be near-zero and replaced with predetermined small value that is tuned to the problem. The second step of the verification of the realizable state is a little more complex. In this stage the check preformed is done in order to validate the full reliability of the PGM as per the conditions derived Section 3.4. For the PGM to admit a realizable state it is critical that the obtained closure coefficients respect the maximum-entropy state and as such the state of the PGM admit a set a hyperbolic PDEs. This check is preformed in a expensive yet robust manner by verifying the eigenvalues of the PGM as presented in Eq. (4.46). The eigenvalue decomposition is preformed on the closure coefficients of the PGM in the following manner,

$$\mathbf{A} = \boldsymbol{L}\Lambda\boldsymbol{L}^{-1}\,, \tag{7.7}$$

where $\mathbf{A}$ is the tensor of closure coefficients expressed as

$$\mathbf{A} = \begin{bmatrix} p_{xx}\, p_{xy}\, p_{xz}\, q_{zs} \\ q_{xy}\, p_{yy}\, p_{yz}\, q_{zs} \\ q_{xz}\, p_{zy}\, p_{zz}\, q_{zs} \\ q_{xs}\, p_{zs}\, p_{zs}\, r_{ss} \end{bmatrix}\,. \tag{7.8}$$

The obtained eigenvalues are related to the principle stresses of the tensor in Eq. (4.46)

$$\mathbf{\Lambda} = \begin{bmatrix} \tilde{p}_{xx}\, \tilde{p}_{yy}\, \tilde{p}_{zz}\, \tilde{r}_{ss} \end{bmatrix}\,, \tag{7.9}$$

and must remain positive in order to ensure the hyperbolicity of the PGM. As such the eigenvalue decomposition, Eq. (7.7) is preformed on very cell and the obtained eigenvalues are then compared to a set tolerance value that is again tuned to the problem in question. If a eigenvalue is found to be less than the set tolerance is it replaced by a small, near zero value and the closure coefficients are then reconstructed with the new eigenvalues, Eq. (7.7). This act of preforming an eigenvalue decomposition then a reconstruction of the $\mathbf{A}$ matrix ensures that the corrected closure coefficients still closely resemble its state prior to the fix but now strictly contains positive eigenvalues such that it respects the hyperbolicity of the PGM.

Chapter 8

Conclusions

8.1 Summary

This thesis presents the use of moment-based methods derived from kinetic theory of gases in order to model polydisperse multiphase flows. The derivation and analysis of a new, surface-weighted model for the efficient prediction of polydisperse multiphase flows is presented and is compared to a previously constructed moment-based model used in order to describe polydisperse multiphase flows. These models belong to the family of Polydisperse Gaussian Models (PGM). In the previous model, the logarithm of the particle diameter is used to differentiate particle sizes, while, in the currently proposed model, particle surface area is used. Regular and surface-weighted velocity moments are presented and used. Both models lead to first-order balance laws and are shown to be robustly hyperbolic. The surface-weighted version of the PGM is demonstrated to exactly recover the correct state for particles settling in a quiescent background. This is thought to be important for several practical problems, namely those present in atmospheric dispersion of particles where the distance and location of the particles as they settle in space is what these models are attempting to predict. However, the surface-weighted version of the closure brings added complexity and numerical difficulties that are not present in the original log-diameter version of the closure. Results obtained, in a space-homogeneous case for both the previous diameter-based PGM and surface-weighted PGM are compared with a kinetic solver. This case is used to illustrate the importance of using surface-based statistics in order to accurately describe the recovery of the correct steady-state solution. Additionally, the three-dimensional case of a settling puff of particles in a cross wind is shown in order to compare both PGM variants to each other in order to investigate their similarities and differences.

8.2 Future Work

While the surface-based PGM shows a promising avenue in the PGM family of models much work still needs to be done in order to build a robust and usable model. Namely, investigation into the surface-based PGM has shown the numerical difficulties one might encounter when implementing a new PGM model using strictly positive distinguishing variables. Many numerical

properties of the diameter-based PGM such as the wavespeeds being known in closed form, and the simpicity of conversion from the moments to the closure-coefficients do not carry over to the surface-based PGM. This means many alternative techniques had to be applied to this new variant of the PGM. Theses techniques, such as using algorithmic differentiation in order to evaluate the wavespeeds at each time step for each cell in the system becomes extremely costly as one increases the number of cells in the simulation. Having to compute the wavespeeds, in addition the Newton-Raphson method in order to convert from the moments to the closure-coefficients being preformed in each cell in the domain leaves much room for improvement.

This thesis only presented a narrow view into the possibility of the set of PGM type models that can be constructed in order to be used for a wide range of various engineering applications. As the need for new models grows the family of PGM can be expanded to cover a wide range of problems. Most notability, the set distinguishing variables can be expanded to consider other properties of the particles. These properties, can be altered to consider a range of different applications such as the particle electric change, the internal temperature, its radioactive charge or viral load. In conjunction with expanding the set of distinguishing variables the source term can also be modified in order to capture how these new distinguishing variables might change due to physics that one might want to capture in the model. With all these factors combined the PGM type of models becomes a strong modular modeling tool able to adjust to any new problem.

Bibliography

[1] Árpád Baricz. "Mills' ratio: Monotonicity patterns and functional inequalities". In: *Journal of Mathematical Analysis and Applications* 340 (2 Apr. 2008), pp. 1362–1370. ISSN: 10960813.

[2] T. J. Barth. "On Discontinuous Galerkin Approximations of Boltzmann Moment Systems with Levermore Closure". In: *Comp. Meth. Appl. Mech. Engrg.* 195 (2006), pp. 3311–3330.

[3] Dean R. Dickinson and W. R. Marshall Jr. "The rates of evaporation of sprays". In: *AIChE Journal* 14.4 (1968), pp. 541–552.

[4] Pingyi Fan. "New inequalities of Mill's ratio and Its Application to The Inverse Q-function Approximation". In: (Dec. 2012). URL: http://arxiv.org/abs/1212.4899.

[5] François Forgues, Lucian Ivan, and Alexandre Trottier. "A Gaussian moment method for polydisperse multiphase flow modelling". In: *Journal of Computational Physics* 398 (Dec. 2019). ISSN: 10902716.

[6] R.O. Fox, F. Laurent, and M. Massot. "Numerical simulation of spray coalescence in an Eulerian framework: Direct quadrature method of moments and multi-fluid method". In: *Journal of Computational Physics* 227.6 (2008), pp. 3058–3088. ISSN: 0021-9991.

[7] Armengol Gasull and Frederic Utzet. "Approximating Mills ratio". In: (July 2013).

[8] Walter Gautschi. "Efficient Computation of the Complex Error Function". In: *SIAM Journal on Numerical Analysis* 7.1 (1970), pp. 187–198. ISSN: 00361429. URL: http://www.jstor.org/stable/2949591.

[9] G.A.E. Godsave. "Studies of the combustion of drops in a fuel spray the burning of single drops of fuel". In: *Symposium (International) on Combustion* 4.1 (1953). Fourth Symposium (International) on Combustion, pp. 818–830. ISSN: 0082-0784.

[10] H. Grad. "On the Kinetic Theory of Rarefied Gases". In: 2 (1949), 331–407.

[11] A. Harten, P. D. Lax, and B. van Leer. "On Upstream Differencing and Godunov-Type Schemes for Hyperbolic Conservation Laws". In: 25.1 (1983), pp. 35–61.

[12] W.C. Hinds. *Aerosol Technology: Properties, Behavior, and Measurement of Airborne Particles*. Wiley, 1999. ISBN: 9780471194101.

[13] s. L. Brown, P. L. Roe, and C. P. T. Groth. *Numerical Solution of a 10-Moment Model for Nonequilibrium Gasdynamics*. Paper 95-1677. AIAA, 1995.

[14] Arthur H Lefebvre and Vincent G McDonell. *Atomization and sprays*. English. OCLC: 1060577045. 2017. ISBN: 9781498736251 9781498736268 9781315120911 9781351637732.

[15] C David Levermore. *Moment Closure Hierarchies for Kinetic Theories*. 1996.

[16] C. David Levermore and W. J. Morokoff. "The Gaussian Moment Closure for Gas Dynamics". In: *SIAM J. Appl. Math.* 59.1 (1998), pp. 72–96.

[17] D. Marchisio and R. Fox. "Solution of population balance equations using the direct quadrature method of moments". In: *Journal of Aerosol Science* 36 (2005), pp. 43–73.

[18] J. G. McDonald, J. S. Sachdev, and C. P. T. Groth. "Application of Gaussian Moment Closure to Micro-Scale Flows with Moving and Embedded Boundaries". In: *AIAA J.* 52 (2014), pp. 1839–1857.

[19] Ingo Müller and Tomasso Ruggeri. *Rational Extended Thermodynamics*. Vol. 37. Springer New York, 1998. ISBN: 978-1-4612-7460-5.

[20] Marco Petrella, Remi Abgrall, and Siddhartha Mishra. "On the discrete equation model for compressible multiphase fluid flows". In: (Apr. 2022). URL: http://arxiv.org/abs/2204.01083.

[21] Iosif Pinelis. "Exact bounds on the inverse Mills ratio and its derivatives". In: (Nov. 2015).

[22] G. P. M. Poppe and C. M. J. Wijers. "More Efficient Computation of the Complex Error Function". In: *ACM Trans. Math. Softw.* 16.1 (Mar. 1990), 38–46. ISSN: 0098-3500. DOI: 10.1145/77626.77629. URL: https://doi.org/10.1145/77626.77629.

[23] J. Wuttke S. G. Johnson. *libcerf*. 2021 [Online]. URL: https://jugit.fz-juelich.de/mlz/libcerf.

[24] R. Saurel, E. Daniel, and J. C. Loraud. "Two-Phase Flows: Second-Order Schemes and Boundary Conditions". In: 32.6 (1994), pp. 1214–1221.

[25] Haim Shore. *Simple Approximations for the Inverse Cumulative Function, the Density Function and the Loss Integral of the Normal Distribution*. 1982, pp. 108–114. URL: https://about.jstor.org/terms.

[26] Christopher G. Small. *Expansions and Asymptotics for Statistics*. Chapman and Hall/CRC, May 2010. ISBN: 9781420011029.

[27] Y. Suzuki and B. van Leer. *Application of the 10-Moment Model to MEMS Flows*. Paper 2005-1398. AIAA, 2005.

[28] A. Vié, F. Doisneau, and M. Massot. "On the Anisotropic Gaussian velocity closure for inertial-particle laden flows". In: 17.1 (2015), pp. 1–46.

[29] Pauli Virtanen et al. "SciPy 1.0: Fundamental Algorithms for Scientific Computing in Python". In: *Nature Methods* 17 (2020), pp. 261–272. DOI: 10.1038/s41592-019-0686-2.

[30] Aymeric Vié, François Doisneau, and Marc Massot. "On the Anisotropic Gaussian Velocity Closure for Inertial-Particle Laden Flows". In: *Communications in Computational Physics* 17.1 (2015), 1–46. DOI: 10.4208/cicp.021213.140514a.

[31] C. Yuan and R.O. Fox. “Conditional quadrature method of moments for kinetic equations”. In: *Journal of Computational Physics* 230.22 (2011), pp. 8216–8246. ISSN: 0021-9991.

[32] Mofreh R. Zaghloul and Ahmed N. Ali. “Algorithm 916: Computing the Faddeyeva and Voigt Functions”. In: *ACM Trans. Math. Softw.* 38.2 (Jan. 2012). ISSN: 0098-3500. DOI: 10.1145/2049673.2049679. URL: https://doi.org/10.1145/2049673.2049679.